Eur. Phys. J. B **38**, 581–598 (2004)
DOI: 10.1140/epjb/e2004-00155-4

THE EUROPEAN PHYSICAL JOURNAL B

Spin-Peierls lattice fluctuations and disorders in $CuGeO_3$ and its solid solutions

J.-P. Pouget[1,a], S. Ravy[1], J.P. Schoeffel[1], G. Dhalenne[2], and A. Revcolevschi[2]

[1] Laboratoire de Physique des Solides, CNRS-UMR 8502, Université Paris-Sud, bâtiment 510, 91405 Orsay Cedex, France
[2] Laboratoire de Chimie de l'État Solide, CNRS-UMR 8648, Université Paris-Sud, bâtiment 414, 91405 Orsay Cedex, France

Received 22 December 2003
Published online 8 June 2004 –

Abstract. The inorganic quasi-one dimensional (1D) $S = 1/2$ antiferromagnetic (AF) system $CuGeO_3$ undergoes a 2nd order spin-Peierls (SP) phase transition at $T_{SP} = 14.2$ K. In this study we present an X-ray synchrotron radiation investigation which confirms that the SP instability is announced by an important regime of pretransitional structural fluctuations which have been detected until 36 K. Furthermore we show that these fluctuations are 1D above 24 K, a feature expected for a structural instability triggered by the Cu^{2+} chains of spin 1/2. By extrapolating the thermal dependence of the correlation length in the chain direction, we show that formation of singlet dimers begins at about 50 K, a temperature that we identify as the mean field temperature of the SP chain. The critical nature of the pretransitional fluctuations does not change when low amounts (<1%) of non-magnetic dopants substitute either the Cu site (case of Zn and Mg) or the Ge site (case of Si and Al) of $CuGeO_3$. However, the spatial extension of the fluctuations is considerably reduced when the magnetic dopant Ni substitutes the Cu site. In the SP ground state of doped materials we have been able to detect, in addition to the superlattice SP reflections previously observed, a very weak anisotropic diffuse scattering. We give evidences that this scattering originates from dopant-induced quasi-1D domains in which the dimerisation is perturbed. If we assume that each domain is limited by a soliton-antisoliton pair, pinned either on the substituent of the Cu site or by the deformation field induced by the substituent of the Ge site, we deduce that the soliton and antisoliton are separated by a distance of about $L_0 \sim 28-45$ Å, and that the soliton half width amounts to about $\xi_{SP} \sim 16-20$ Å. With these numbers we are able to account for the rate of decrease of T_{SP} as a function of the dopant concentration, and to deduce the critical concentration above which the long-range SP order vanishes. The overall size of the perturbed domains thus obtained, $L_0 + 2\xi_{SP} \sim 70$ Å, is comparable with the size of the magnetic inhomogeneities determined by muon spin spectroscopy in the AF phase of doped $CuGeO_3$.

PACS. 71.27.+a Strongly correlated electron systems; heavy fermions – 61.72.Dd Experimental determination of defects by diffraction and scattering – 75.45.+j Macroscopic quantum phenomena in magnetic systems

1 Introduction

One of the major achievements of solid state physics studies of the end of the 20th century was the discovery of quantum cooperative phenomena [1] which tend to promote collective behaviour such as superconductivity, charge, spin or orbital density waves, together with charge or spin gapped states [2]. These features are particularly well documented in systems of reduced electronic or magnetic dimensionality [3]. The description of these quantum ground states and of their phase diagram when external parameters such as pressure, magnetic field or chemical composition is varied, is one of major issues of to day studies.

Among these systems quantum one-dimensional (1D) antiferromagnetic (AF) spin chains and ladders have been particularly studied [4]. The main reason is that their ground state properties do not vary continuously when either the spin S of the chain or the number of legs in the ladder changes. For example, the $S = 1/2$ chain develops at $T = 0$ K local AF correlations due to quantum fluctuations [4], while the $S = 1$ chain exhibits a non-magnetic singlet ($S = 0$) ground state with a finite gap in its spin excitation spectrum [3]. An $S = 1/2$ spin ladder with an odd number of legs behaves as the $S = 1/2$ AF chain, while an $S = 1/2$ spin ladder with an even number of legs behaves as the $S = 1$ AF chain [4]. Even for an $S = 1/2$ AF chain, an important fraction of the ground state fluctuations contains non-magnetic singlet components. These components can be picked out of the quantum fluctuations in presence of a sizeable spin-phonon coupling allowing the chain to dimerize [5]. This gives rise to a spin-Peierls (SP) phase transition where, below T_{SP}, the dimerisation achieves a lattice of non-magnetic $S = 0$ singlet pairs, whose magnetic excitations are separated by a gap Δ from

[a] e-mail: pouget@lps.u-psud.fr

the ground state. Spin gapped ground states occur for a wide class of $S = 1/2$ AF chains including the XXY chain with second neighbour exchange interactions [6] and where the gap is achieved by frustration effects between first (J) and second (J') neighbour AF exchange interactions. In such a case, the physics of the spin chain is dominated at short distance by spin singlet formation. Its dynamics is such that a given spin spends half of its time forming a singlet with its right partner and the other half of the time with its left partner, a feature which recalls the "resonating valence bond" (RVB) picture pointed out 30 years ago by Anderson [7].

The formation of such a spin gap is a remarkable phenomenon since a macroscopic number of spins becomes quenched. This state is however very sensitive to perturbations: for example, a small amount of non-magnetic substituents releases "unpaired" 1/2 spins which will thus develop local AF correlations [8] decreasing exponentially in space. The non-gapped phase can be recovered by applying a magnetic field larger than Δ. For SP systems, the magnetic field stabilizes an incommensurate lattice of solitons where each discommensuration (which bears an $S = 1/2$ moment decorated with AF correlations) separates two neighbouring regions where the phase of the dimerisation jumps by π [9].

It was often argued that the SP transition of a $S = 1/2$ AF chain is the analogue of the Peierls transition of a metallic chain. In fact, the SP transition is analogous to the Peierls transition in a spinless fermion gas. Its main consequence is that the SP ground state is achieved only for a strong enough spin-phonon coupling α [10,11], while the conventional Peierls ground state exists whatever the strength of the electron-phonon coupling. For smaller values of α (for $\alpha < 0.6\Omega_0$, if $\Omega_0 < 2J$, according to Ref. [11]), the quantum fluctuations destroy the SP dimerised ground state. In the SP ground state, the importance of quantum effects depend on the relative values of the microscopic interactions, such as the spin-phonon coupling α, the first neighbour exchange interaction J and the bare frequency of the critical phonon mode Ω_0 [10]. In a critical analysis of the experimental situation we have shown [12] that organic salts such as $(TMTTF)_2X$ and $(BCPTTF)_2X$, with $X = PF_6$ and AsF_6, belong to the classical region while the organic salts MEM-$(TCNQ)_2$, and probably TTF-CuBDT, are at the boundary between classical and quantum regions and that the inorganic cuprate $CuGeO_3$ belongs to the quantum region. These different regimes are conditioned by the adiabatic or non-adiabatic nature of the coupling between the spin and structural degrees of freedom at the origin of the SP instability. For example, the critical softening of the frequency of a phonon mode, in the adiabatic limit, leads to the formation of a pseudo gap in the spin degrees of freedom [13,14]. It is now well established that there is no phonon mode softening in $CuGeO_3$ [42] and that the non-adiabatic limit is relevant to describe its physical properties [15]. The important question of the dynamics of the SP transition (existence of a soft mode or/and of a central peak in energy), has already been considered in reference [12]. Here we shall not address this question because X-ray diffuse scattering, which integrates the fluctuations in energy, does not bring any information concerning the dynamics of the pretransitional fluctuations.

Table 1. Oxidation state, ionic radius (in Å) and spin state of the M = Zn, Mg, Ni and T = Si, Ti, Al substituents of the Cu and Ge of $CuGeO_3$, respectively.

	Cu^{2+}	spin	Ge^{4+}
$CuGeO_3$	0.87	1/2	0.53
Substituent	M		T
M^{2+} = Zn	0.88	0	
Mg	0.86	0	
Ni	0.83	1	
T^{4+} = Si		0	0.40
Ti		0	0.56
T^{3+} = Al	Cu^{3+}	1	0.53
	or Zang & Rice singlet	0	

However, X-ray diffuse scattering brings invaluable informations concerning the anisotropy of these fluctuations. In the case of $CuGeO_3$ we have shown [16,17] that the SP transition is announced by a sizeable regime of 1D pretransitional fluctuations, as expected for a structural instability triggered by the magnetic 1D subsystem. Here, and this is the first purpose of this paper, we complete these results by a synchrotron radiation study allowing to define more accurately the dimensionality of the critical fluctuations of $CuGeO_3$ and their temperature range of existence above T_{SP}. A brief report of this work had already appeared in reference [18].

The $CuGeO_3$ system allows to study experimentally, for the first time, the influence of defects on the SP ground state. As mentioned above, it is expected, on theoretical grounds, that defects will depair 1/2 spins of the SP chain which will thus develop local AF correlations. In this respect, it has been shown that, while the pure material exhibits only a long range SP dimerisation below $T_{SP} = 14.2$ K, there is a coexistence between the 3D-SP distortion and the 3D-AF long-range order in substituted $CuGeO_3$ for vanishing small concentrations of substituents both on the Cu and Ge sites [19]. The phase diagram of substituted $CuGeO_3$ is now well established experimentally [20–22], but the manner by which the AF order locally nucleates upon doping, is not really known, although several theories [23–28] have addressed this question. In this study, and this is the the second purpose of this paper, we report the first determination of the microstructure of the SP ground state in presence of substituents. In this respect, we complete a previous study [17] of the influence of the substituents on the SP instability of $CuGeO_3$.

2 Experimental conditions

2.1 Samples

The experiments have been conducted both on pure $CuGeO_3$ and substituted $Cu_{1-x}M_xGe_{1-y}T_yO_3$ samples, with M = Zn, Mg, Ni or T = Si, Ti, Al. Table 1 indicates the oxidation state, the ionic radius and the spin state of these substituents. Among the substituents there is a large

Table 2. Spin-Peierls critical temperature, T_{SP}, rate of decrease of T_{SP} with the dopant, anisotropy of the inverse correlation lengths and 3D-2D crossover temperature of the pretransitional critical fluctuations in pure and substituted $CuGeO_3$. * deduced from this study and of reference [32]. ** deduced from the measurements of reference [33] very close to T_{SP}.

	T_{SP}(K)	dT_{SP}/dx (K/%)	$\xi_a^{-1} : \xi_b^{-1} : \xi_c^{-1}$	T_{3D-2D}(K)
Pure	14.25(10)		$7 : 2.5 : 1^*$	16
			$5 : 3 : 1^{**}$	
M substituent				
$x = 0.6\%$ Zn	13.0(1)	−2.1(3)	4 : 2.7 : 1	
$x = 0.8\%$ Mg	12.9(1)	−1.7(3)	5 : 2 : 1	14.7
$x = 0.9\%$ Ni	13.15(10)	−1.2(3)	2 : 0.7 : 1	13.6
T substituent				
$x = 0.1\%$ Si	13.7(1)	−5.5(20)	? : 1.7 : 1	
$x = 0.3\%$ Si	12.5(1)	−5.8(7)		
$x = 0.2\%$ Al	13.4(1)	−4.2(10)	6 : 2.7 : 1	15.7
$x = 0.4\%$ Ti	14.0(1)	−0.6(5)	? : 2.6 : 1	

difference of size between Si^{4+} and Ge^{4+}, the Al^{3+} substituent is not isoelectronic with the Ge^{4+}, and the Ni^{2+} substituent is magnetic.

The single crystals studied were grown from the melt by a floating-zone method associated with an image furnace [29]. The determination of the substituent content of the crystals was made by inductively coupled plasma atomic-emission spectroscopy (ICP/AES) [30]. Table 2 gives the concentration of the various samples investigated.

The $CuGeO_3$ single crystal studied here was different from the one investigated in references [16,17]. The Si, Zn, Mg and Ni substituted $CuGeO_3$ single crystals are from batches used in the studies of references [20,22]. The single crystals have the form of (b, c) platelets of a few 10 μm of thickness along a- and of a few mm in the b- and c-directions. They were cleaved from larger centimeter size single crystals.

2.2 X-ray scattering conditions

The study of the SP pretransitional fluctuations of pure $CuGeO_3$ was performed at the D2AM (BM2) beamline of the European Synchrotron Radiation Facility (ESRF) with an X-ray energy of 8 keV. The experimental resolution, determined by the half width at half maximum (HWHM) of the (1, 1, 1) main Bragg reflection, was $\Delta Q_a = 0.01$ Å^{-1}, $\Delta Q_b = 0.009$ Å^{-1} and $\Delta Q_c = 0.006$ Å^{-1} along the three orthogonal directions scanned (a, b and c respectively). A very weak diffuse scattering was observed at the (3/2, 1, 3/2) and (1/2, 1, 3/2) reciprocal positions. Due to the broadness of the diffuse scattering in the temperature range studied (19–36 K), the fit of the profile of the peaks was performed with a Lorentzian line shape (which Fourier transform corresponds to fluctuations which decay exponentially in real space) without applying any deconvolution procedure.

The investigation of the SP transition in the $Cu_{1-x}M_xGe_{1-y}T_yO_3$ crystals was performed with a home-made three circle diffractometer (normal beam geometry with a lifting scintillator detector) mounted on a rotating anode X-ray generator operating at 55 kW, 180 mA and providing the Cu-Kα ($\lambda = 1.542$ Å) radiation after (002) reflection of the incoming beam on a doubly bent pyrolitic graphite monochromator. The experimental conditions were the same as those of the previous study of reference [17]. In particular, the experimental resolution, given by the HWHM of the main Bragg reflection (ΔQ_i), is about 3 times larger than that of the D2AM synchrotron radiation study. For each alloy investigated, the (3/2, 1, 3/2) satellite reflection was followed from ∼11 K to T_{SP}. Very weak pretransitional fluctuations were observed in a temperature range of a few K above T_{SP}. They were measured along the a, b and c crystal directions.

In the 0.1% Si crystal, the (3/2, 2, 3/2) satellite reflection, due only to the staggered rotation of the CuO_2 square in the SP phase [31], was also observed, but with an intensity 25 times smaller than that of the (3/2, 1, 3/2) satellite reflection. Thus the X-ray study performed in the vicinity of the (3/2, 1, 3/2) reciprocal position of pure and substituted $CuGeO_3$, which will be reported below, probes mainly the SP polarisation associated with the dimerisation of the Cu chains.

In the substituted crystals, a very weak and broad X-ray diffuse scattering was also detected below T_{SP} in addition to the SP superlattice reflections. Its detection was essentially performed at 10.5 K with the fixed film-fixed crystal method in the conditions described in references [16,17]. In particular, X-ray patterns were taken with a conventional generator providing the Cu-Kα radiation and operating at 15 kV, in order to avoid the $\lambda/2$ contamination from the continuous spectrum of the X-ray tube.

3 Experimental results

3.1 The pretransitional spin-Peierls fluctuations of $CuGeO_3$

The purpose of our synchrotron radiation investigation was the measurement of the pretransitional fluctuations of the SP transition of $CuGeO_3$ far from T_{SP} because their synchrotron radiation study in the near vicinity of T_{SP} has already been reported in references [32,33]. Figure 1

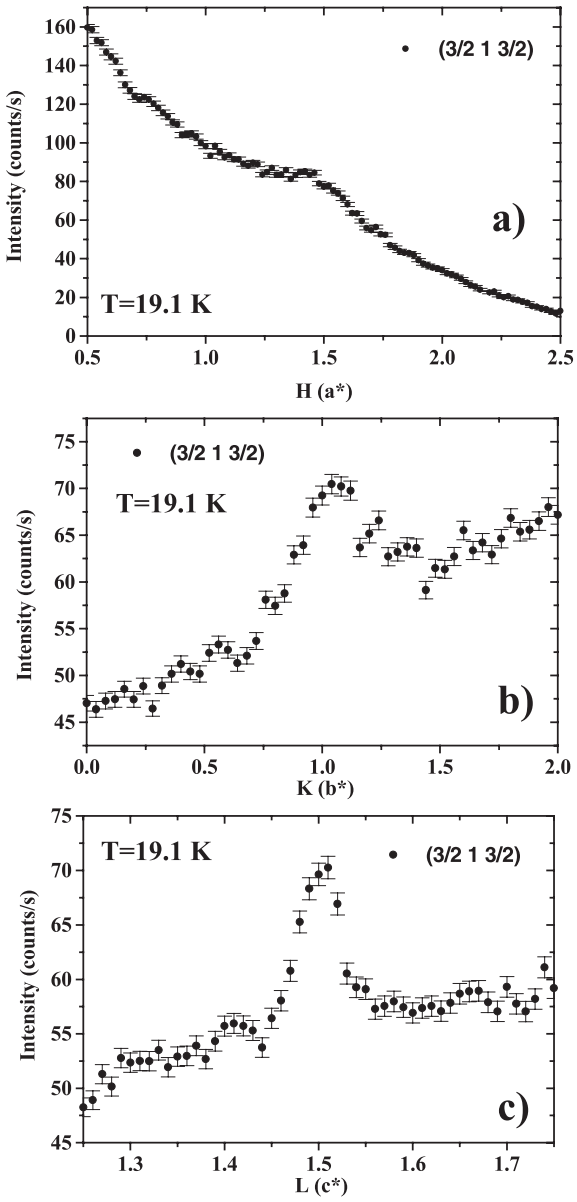

Fig. 1. Scans along the a^*, b^* and c^* reciprocal directions of the X-ray diffuse scattering of $CuGeO_3$ at 19.1 K around the (3/2, 1, 3/2) reciprocal position.

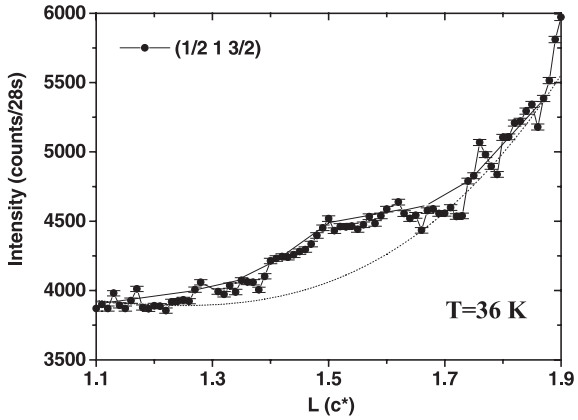

Fig. 2. Scan along the c^* reciprocal direction of the X-ray diffuse scattering of $CuGeO_3$ at 36 K around the (1/2, 1, 3/2) reciprocal position. The continuous line is a fit of the excess of intensity of the diffuse scattering above the background (dotted line) by a Lorentzian profile.

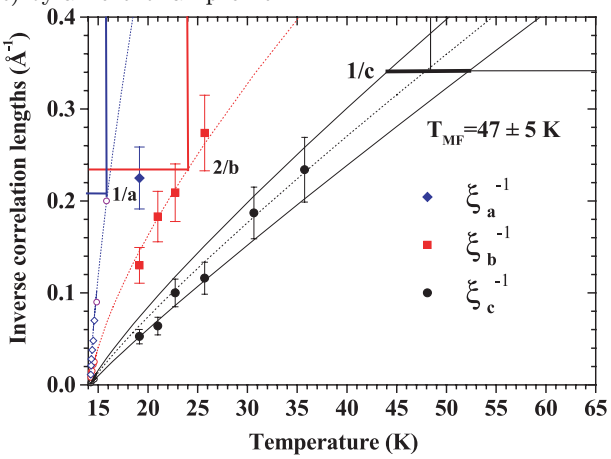

Fig. 3. Thermal dependence of the inverse correlation lengths ξ_a^{-1}, ξ_b^{-1} and ξ_c^{-1} in $CuGeO_3$. This figure defines the 3D-2D crossover temperature when $\xi_a^{-1} = 1/a$ and the 2D-1D crossover temperature when $\xi_b^{-1} = 2/b$, and T_{MF} when $\xi_c^{-1} = 1/c$. The solid symbols are from the present study and, in the vicinity of T_{SP}, the open symbols from the data of references [32,33]. The lines are power law dependence adjusted on the data in the vicinity of T_{SP}.

presents, at 19.1 K (the lowest temperature studied), scans of the pretransitional fluctuations along the a, b and c orthorhombic directions. They clearly show, in agreement with previous reports [17,33], that the SP fluctuations of $CuGeO_3$ are quite anisotropic. The inverse correlation lengths, ξ^{-1}, obtained from the HWHM of the Lorentzian profile of the diffuse scattering, are for the scans shown in Figure 1:

$$\xi_c^{-1} = 0.052 \text{ Å}^{-1} < \xi_b^{-1} = 0.13 \text{ Å}^{-1} < \xi_a^{-1} = 0.22 \text{ Å}^{-1}.$$

The correlation length is the longest in the magnetic chain direction, c, as expected for a structural transition trigged by the spin subsystem. In the c-direction, the pretransitional fluctuations have been measured until 36 K (Fig. 2). At this temperature, one measures $\xi_c^{-1} \approx 0.23$ Å^{-1}, a value comparable the one obtained at 40 K in the photographic investigation of reference [16], but two times larger than the one obtained at 35 K in the diffractometric investigation of reference [17]. At 19.1 K (Fig. 1) and 36 K (Fig. 2), the X-ray diffuse scattering has respectively a peak intensity of about 23% and 10% of the background (against 7% and 4% at about the same temperatures in the study performed with a conventional X-ray generator in Ref. [17]). With a diffuse scattering having a better signal to noise ratio, our ξ_i^{-1}'s determination is thus more accurate than the one given in our previous investigation of reference [17].

Finally, Figure 3 gives the thermal dependence of the ξ_i^{-1}'s. This figure includes also the synchrotron radiation measurements performed in the near vicinity

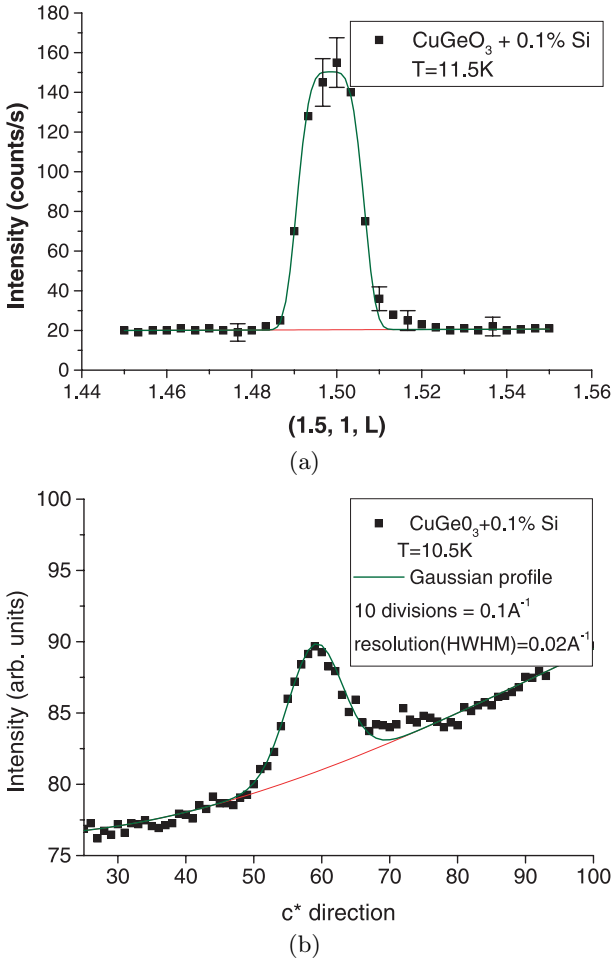

Fig. 4. Scans along the c^* reciprocal direction of the 0.1% Si sample of: (a) the (3/2, 1, 3/2) satellite reflection at 11.5 K, and (b) of the residual diffuse scattering at the (h, 1, 3/2) reciprocal position, shown by the upper arrow in Figure 8b, at 10.5 K. In (a) the profile has been fitted by a Gaussian squared (resolution function of the diffractometer) and in (b) by a Gaussian. Note the asymmetry of profile of the superlattice reflection and of the diffuse scattering for large l values.

of T_{SP} [32,33]. Our ξ_i^{-1}'s values are in the continuation of these data, if one assumes a critical behaviour under the form of a power law in temperature. The ξ_c^{-1}'s values found in the present investigation slightly differ from those obtained in our earlier low resolution study [17], performed with a different $CuGeO_3$ crystal.

3.2 The spin-Peierls transition and the pretransitional fluctuations of $Cu_{1-x}M_xGe_{1-y}T_yO_3$

In all the crystals investigated, and containing a small amount of substituent $x < 1\%$ (or $y < 0.5\%$) on the Cu (or Ge) site (see Tab. 2), a well-defined SP transition was detected from the growth of sharp superlattice satellite reflections. Its critical temperature, T_{SP}, which depends on the amount of substituent, is quoted in Table 2. A typical scan along c^* of the (3/2, 1, 3/2) SP reflection of the 0.1% Si sample is shown Figure 4a. This reflection has the profile and the width of the experimental resolution ($\Delta Q_c = 0.017$ Å^{-1}; HWHM). At the scale of this experimental resolution, the crystal undergoes a SP order exceeding 160 Å (i.e. $0.888\pi/\Delta Q_c$ — see Sect. A.3 of the Annexe) in the c-direction. Similar results were found in all the samples which were investigated. The only case where satellite reflections broader than the experimental resolution were measured was the 0.6% Zn sample previously investigated in reference [17]. However, sharp satellite reflections were apparently observed for a 1% Zn sample in another study [33].

Above T_{SP}, the sharp satellite reflections transform into a weak diffuse scattering broader than the experimental resolution. Typical scans along the a^*-, b^*- and c^*-directions around the (3/2, 1, −3/2) reciprocal position of the 0.8% Mg sample are shown in Figure 5. This diffuse scattering becomes critical as T_{SP} is approached from above, as expected for a 2nd order phase transition.

Figure 6 gives, for the 0.3% Si sample, the thermal dependence of the X-ray peak intensity at the (3/2, 1, −3/2) reciprocal position. The peak intensity (I) of the X-ray diffuse scattering in excess of the background diverges critically at T_{SP}. This is more clearly illustrated in the insert of this figure which shows that the inverse of this quantity, corrected by the thermal population factor, T/I, follows a linear Curie-Weiss type dependence in $T - T_{SP}$. Its extrapolation to zero leads to $T_{SP} = 12.5$ K.

After deconvolution with the experimental resolution, the HWHM of the diffuse spots gives the inverse correlation length, ξ_i^{-1}, of the pretransitional fluctuations in the scan direction (i). The critical divergence of the fluctuations leads to a vanishing of ξ_i^{-1} at T_{SP}. Figure 7 shows the thermal dependence, both of the peak intensity and of the inverse correlation length ξ_i^{-1} of the 0.8% Mg (Fig. 7a), 0.2% Al (Fig. 7b) and 0.9% Ni (Fig. 7c) samples. The vanishing of the inverse correlation lengths allows to deduce that T_{SP} occurs respectively at 12.9 K, 13.4 K and 13.15 K. Our T_{SP} value for the 0.8% Mg sample is higher than the one, of 11 K, given in reference [34] for a sample of same concentration.

Table 2 summarizes, for all the samples investigated, the critical temperature T_{SP} at which the critical fluctuations diverge.

This determination of T_{SP} allows to obtain the rate of decrease of T_{SP} with the dopant concentration x: dT_{SP}/dx. Within experimental errors, Table 2 shows that dT_{SP}/dx is very similar for all the Cu substituents (between −1 and −2 K/% for M = Ni, Mg and Zn). But the rate of decrease is much smaller than for the Ge substituents (between −4 and −6 K/% for T = Al and Si). The rate of decrease of T_{SP} for the Mg and Zn samples is in good agreement with the one, $-\{1.8{-}2.1\}$ K/%, determined from the drop of the magnetic susceptibility in references [21,22,35]. T_{SP} is depressed by only 1 K for the 0.9% Ni sample studied. However for the same Ni content, a smaller value of T_{SP} (12.6 K) is obtained from the magnetic measurements of reference [36]. Thus, one cannot exclude that the real Ni concentration of our

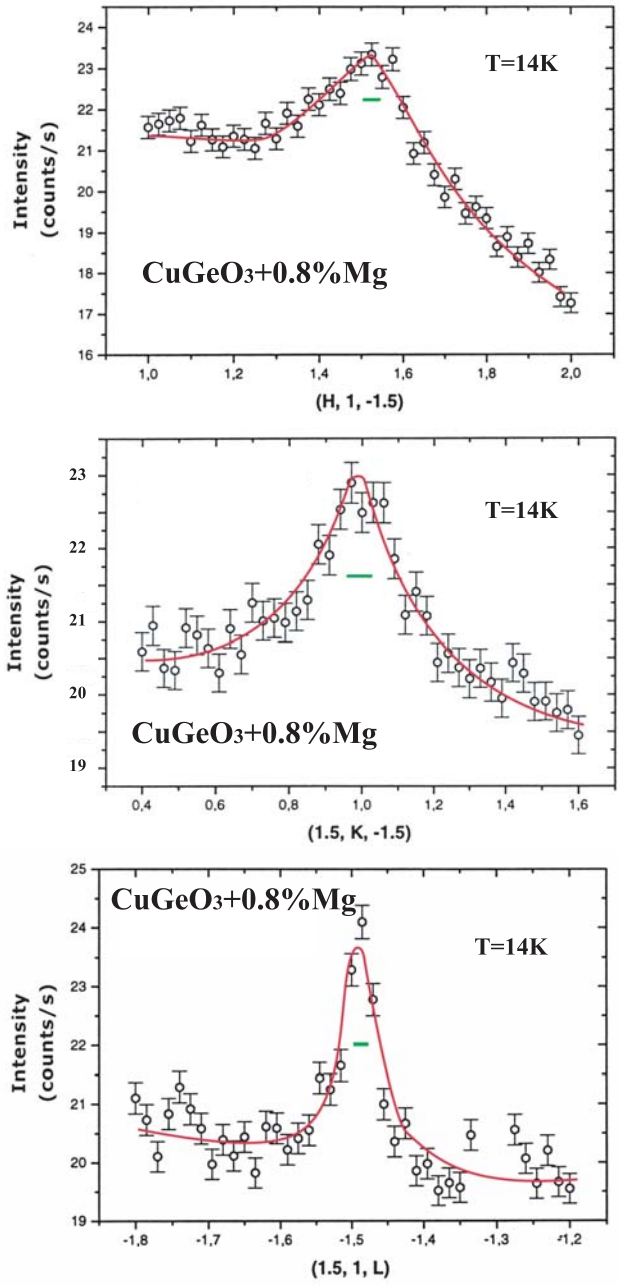

Fig. 5. Scans along the a^*, b^* and c^* reciprocal directions of the X-ray diffuse scattering around the (3/2, 1, −3/2) reciprocal position for the 0.8% Mg sample at 14 K (the horizontal bar represents twice the HWHM of the experimental resolution).

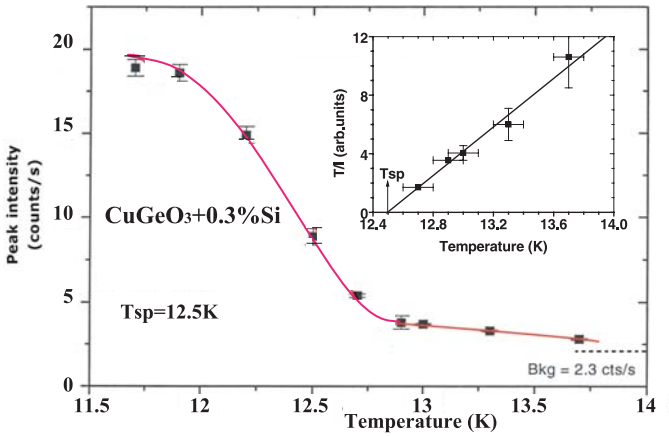

Fig. 6. Thermal dependence of the (3/2, 1, −3/2) satellite peak intensity for the 0.3% Si sample. The insert shows the thermal variation of T/I, a quantity corresponding to the inverse susceptibility, and whose vanishing allows the determination of T_{SP}.

sample was slightly smaller than 0.9%. For the Si samples investigated, the rate of decrease of T_{SP} is in good agreement with the one (−6.3 K/%) determined from the magnetic measurements of reference [20]. The rate of decrease of T_{SP} in our Al sample is 7 times stronger than the one reported in reference [37]. Finally, a very small rate of decrease of T_{SP} is found for the T = Ti substituent, in agreement with to the one determined in reference [37].

Table 2 gives also the anisotropy of the inverse correlation length. Except for the Ni sample, the anisotropy ratio is very similar in all the samples studied and comparable to the one of pure $CuGeO_3$. The anisotropy ratio of the 0.6% Zn sample $\xi_a^{-1} : \xi_b^{-1} : \xi_c^{-1} \approx 4 : 2.7 : 1$ is close to the one, $\xi_a^{-1} : \xi_b^{-1} : \xi_c^{-1} \approx 5.9 : 3 : 1$, reported in a synchrotron radiation study of a 1% Zn sample [33]. The rate of thermal increase of the ξ_i^{-1}'s is also very similar in all the samples studied, except for the Ni one (compare Figs. 3, 7a and 7b). Figure 7c shows that, in the Ni sample, the longest correlation is not along the magnetic chain direction c but along the interchain direction b. In addition, in this sample, the ξ_i^{-1}'s increase extremely rapidly upon heating. For example, Figure 7 shows that 0.5 K above T_{SP}:

- ξ_a^{-1} of the Ni sample is 2.5 (4) times larger than ξ_a^{-1} of the Mg (Al) sample,
- ξ_b^{-1} of the Ni sample is 2 (4) times larger than ξ_b^{-1} of the Mg (Al) sample,
- ξ_c^{-1} of the Ni sample is 4 (10) times larger than ξ_c^{-1} of the Mg (Al) sample.

This proves that ξ_c^{-1} is more strongly affected by the Ni substitution than ξ_a^{-1} and ξ_b^{-1}. The largest increase of ξ_c^{-1} causes the change of anisotropy of the ξ_i^{-1}'s.

3.3 The residual X-ray diffuse scattering in the spin-Peierls phase of $Cu_{1-x}M_xGe_{1-y}T_yO_3$

Figure 8 shows X-ray patterns taken (a) in pure $CuGeO_3$ at 10.6 K and (b) in the 0.1% Si compound at 10.5 K. In pure $CuGeO_3$, only sharp satellite reflections are observed in the SP phase (Fig. 8a), as previously reported [16]. In the 0.1% Si sample, only residual diffuse segments are detected (Fig. 8b) in the SP phase. In the photographic investigation of this latter sample, the crystal was slightly misoriented so that the SP superlattice spots were not put in reflection on the Ewald sphere. With the 0.3% Si sample

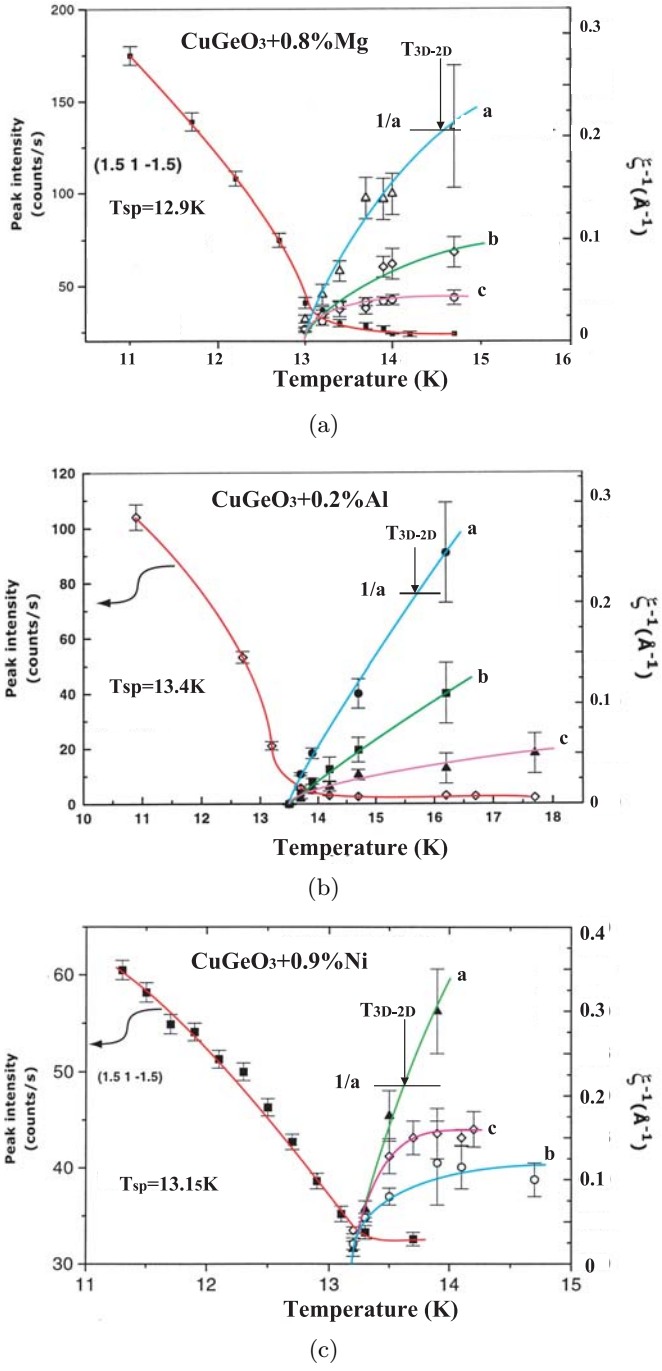

Fig. 7. Thermal dependence of the (3/2, 1, −3/2) satellite peak intensity and of the inverse correlation lengths ξ_a^{-1}, ξ_b^{-1} and ξ_c^{-1} for the (a) 0.8% Mg, (b) 0.2% Al and (c) 0.9% Ni samples. The crossover temperature T_{3D-2D} is indicated.

mounted in a more symmetric manner, the SP satellite reflections could be detected by the photographic investigation, corroborating the results of its diffractometric study. Only the observation of residual diffuse segments was reported in our previous investigation of the Si alloys [17].

For the 0.1% Si sample, Figure 4b presents a microdensitometer reading along the c^*-direction across the

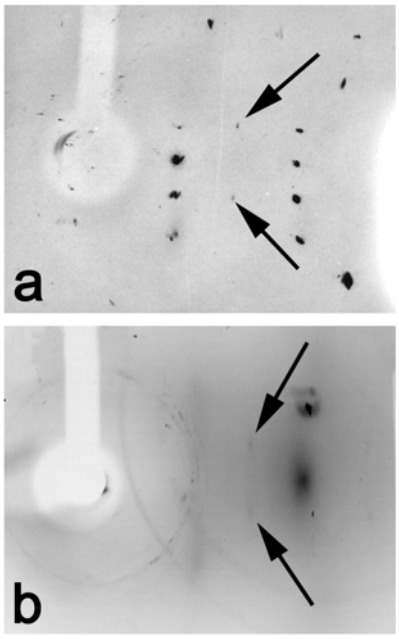

Fig. 8. X-ray patterns of pure $CuGeO_3$ at 10.6 K (a) and of the 0.1% Si-doped sample at 10.5 K (b) taken with about the same sample orientation. The arrows point towards the SP superlattice reflections in (a) and towards the residual SP diffuse scattering in (b). The c^*-direction is horizontal and the b^*-direction is vertical. These X-ray patterns have been taken without $\lambda/2$ contamination.

$l = 3/2c^*$ diffuse line of the X-ray pattern shown Figure 8b. It shows: (1) that along c^* the diffuse line is 2.5 times larger than the experimental resolution, and (2) that its intensity is quite weak (∼12% of the background intensity). A comparison with Figure 4a shows that the peak intensity of the diffuse line is about 50 times less intense than the satellite peak intensity. The weakness of the diffuse scattering (corresponding to about 2.5 counts/s in the intensity scale of Fig. 4a) explains why it could not be detected in the diffractometric investigation of Section 3.2. In addition, the SP superlattice reflections present an asymmetric profile, probably due to the deformation field induced by the Si substituent in the $CuGeO_3$ matrix (whose smaller ionic radius leads to a shrinkage of the lattice parameters) and whose intensity is larger than that of the residual diffuse scattering (see Fig. 4). Thus, only scans slightly off the position of the SP reflections, such as those performed by the microdensitometer reading of long exposure photographs, are able to reveal the residual diffuse scattering.

The HWHM along c^* of the residual diffuse scattering in the SP phase of the 0.1% Si compound, shown Figure 4b, is, after correction with the experimental resolution, of $\Delta Q_c \approx 0.04$ Å^{-1}. Within experimental error (± 0.005 Å^{-1}), this quantity is the same for the 0.25% and 0.5% Si samples already investigated in reference [17]. In these samples, the diffuse scattering intensity is also modulated in the b^*-direction, which indicates that the region perturbed by the dopant involves several chains.

From the values: $\Delta Q_b = 0.11 \pm 0.02$ Å^{-1} obtained in the 0.1% sample, $\Delta Q_b \approx 0.09$ Å^{-1} in the 0.25% Si sample and $\Delta Q_b = 0.11 \pm 0.01$ Å^{-1} in the 0.5% Si sample [17], one deduces, from $\xi_b^P = \Delta Q_b^{-1} \approx b$, that about $n_b = 3$ chains are coupled in the b-direction.

The same photographic investigation has been performed with other doped samples. In the 0.2% Al sample, diffuse lines, slightly modulated along b^*, were also observed below T_{SP}. At 10.5 K, their intrinsic HWHM in the c^* and b^* directions was found to be $\Delta Q_c = 0.04 \pm 0.01$ Å^{-1} and $\Delta Q_b \approx 0.2$ Å^{-1} respectively. From ΔQ_b, one deduces that the perturbed region connects $n_b = 2$ chains in the b-direction ($\xi_b^P \approx b/2$). In the 0.6% Zn sample, already studied in reference [17], diffuse lines are also detected below T_{SP}, with, at 10.5 K: $\Delta Q_c = 0.04 \pm 0.005$ Å^{-1} and no sizeable interchain coupling along b ($\xi_b^P < b/2$).

All these results show that in the SP ground state, the typical size of the perturbed regions in the magnetic chain direction does not significantly depend upon the nature and the concentration of the dopant (for small x and y values at least): It amounts to about $\xi_c^P = (\Delta Q_c)^{-1} \approx 25$ Å. However, the transverse size, in the b-direction, of the perturbed region seems to depend upon the nature of the dopant or, more likely, on the nature of the site which is substituted: interchain correlations along b are observed for the Si and Al substituents of Ge, which is located between the magnetic chains.

4 Discussion

4.1 The spin-Peierls pretransitional fluctuations of $CuGeO_3$ and its solid solutions

In order to define the dimensionality of the structural fluctuations, the transverse correlation length has to be compared with the interchain distance $a = 4.8$ Å or $b/2 = 4.25$ Å. In the data shown Figure 1, ξ_a^{-1} is larger than $1/a = 0.21$ Å^{-1} at 19.1 K, which means that $CuGeO_3$ is already in the regime of 2D fluctuations. Earlier measurements [17,32] have shown that the crossover temperature from 3D to 2D fluctuations, T_{3D-2D}, defined by $\xi_a^{-1} = 1/a$, occurs at about 16 K (∼2 K above T_{SP}) in $CuGeO_3$. From the thermal dependence of ξ_a^{-1} (Fig. 7) we have determined (Tab. 2) T_{3D-2D} for the Mg, Al and Ni substituted crystals. In the 0.8% Mg and 0.2% Al samples, T_{3D-2D} occurs also at about 2 K above T_{SP}. This is not the case for the 0.9% Ni sample for which T_{3D-2D} occurs only 0.5 K above T_{SP}!

The crossover temperature to the regime of 1D fluctuations, T_{2D-1D} defined by $\xi_b^{-1} = 2/b$ has not been determined accurately until now. The data presented Figure 3 allow to determine $T_{2D-1D} \approx 24$ K in $CuGeO_3$. The regime of 1D fluctuations thus starts at T_{SP} +10 K. We have not been able to determine T_{2D-1D} in the substituted compounds because the pretransitional fluctuations are only detectable in the near vicinity of T_{SP}. However in the temperature range investigated, ξ_b^{-1} of all the substituted compounds, except for the Ni one, roughly scales, as a function of the reduced temperature T/T_{SP}, as ξ_b^{-1} of pure $CuGeO_3$. If one assumes that such a scaling law still holds at higher temperatures, one keeps: $T_{2D-1D} \approx T_{SP} + 10$ K. Also, within experimental error, ξ_c^{-1} of the substituted compounds, except for the Ni one, scales in T/T_{SP} with ξ_c^{-1} of pure $CuGeO_3$.

Thus below, we shall discuss separately the behaviour of pure $CuGeO_3$ (and with non magnetic dopant) from that of the Ni substituted sample.

4.1.1 Pure $CuGeO_3$

Above T_{2D-1D}, a regime of 1D SP structural fluctuations takes place in pure $CuGeO_3$. These fluctuations have been detected until 40 K in the photographic investigation of reference [16], 35 K in the diffractometric investigation of reference [17], and 36 K in the present synchrotron radiation study (Fig. 2). If one extrapolates by a power law the thermal dependence of ξ_c^{-1} one finds that ξ_c^{-1} reaches $1/c$ at about 47 ± 5 K (Fig. 3). At this temperature, two neighbouring spins begin to be paired into a dimer. An exact calculation of the structural fluctuations associated with the SP order parameter [14] shows that the preformation of singlet dimers occurs at about the mean field temperature, T_{MF}, of the chain (i.e. the SP transition temperature calculated in the mean field approximation). One thus gets from the present data: $T_{MF} \sim 50$ K. This finding confirms a previous analysis [12] of less accurate measurements of ξ_c which gave a mean-field temperature of $T_{MF} \sim 60$ K. The finding of a T_{MF} as high as 50–60 K agrees with recent NMR and NQR studies of the $CuGe_{1-x}Si_xO_3$ solid solution [65].

It is interesting to note that $T_{MF} \sim 50$ K is very close to the temperature at which the spin susceptibility exhibits a maximum [38]. It is well known that the low temperature decrease of spin susceptibility of the $S = 1/2$ AF chain is due to the growth of AF correlations (i.e. to the development of a short range AF order as shown by Raman measurements in $CuGeO_3$ [39]). In $CuGeO_3$, the SP pretransitional structural fluctuations thus develop jointly with the AF short-range order. The fact that AF fluctuations trigger the structural instability is expected in the mechanism of a true SP instability. However, the nearly coincidence of T_{MF} with the onset of AF correlations requires quite strong spin-phonon interactions. This finding is also consistent with the observation of anomalies at about T_{MF} in the thermal expansion of the lattice parameters of $CuGeO_3$ [40]. These features can be more quantitatively assessed by the deduction of the spin-phonon coupling constant α from T_{MF}, via the Cross and Fischer relationship [41]:

$$k_B T_{MF} = 1.6\alpha^2/\pi\hbar\Omega_0. \quad (1)$$

In $CuGeO_3$, there are two critical phonon modes at $\hbar\Omega_o/k_B = 310$ K and 150 K [42], from which the use of relationship (1) leads to $\alpha \sim 170-120$ K. The coincidence of this value with the near neighbour exchange interaction $J \sim 160$ K of the AF chain [38] shows that $CuGeO_3$ is in the strong coupling situation.

Using the analogue of the BCS relationship for the SP chain [12b]:

$$\Delta_{MF} \approx 2.3\ k_B T_{MF}, \tag{2}$$

one deduces a mean-field SP gap: $\Delta_{MF}/k_B \approx 108$ K. This value is 4 times larger than the singlet-triplet SP gap experimentally measured $\Delta/k_B \approx 28$ K (neutron scattering measurements [43,44] give $\Delta/k_B = 24$ K, at the AF critical wave vector and 31 K, at the SP critical wave vector). It thus appears that there is a strong reduction of the SP gap with respect to its mean field value. Such a reduction can be attributed to quantum fluctuations. Consistently, the fact that $\hbar\Omega_0 > \{\Delta_{MF}, J\}$ shows that $CuGeO_3$ is in the quantum regime [10]. The values $\hbar\Omega_0/k_B = 310$ K, $\alpha \sim 170$ K and $J \sim 160$ K, place $CuGeO_3$ just at the boarderline between the dimerised and uniform (i.e. spin liquid) phases in the phase diagram of the Heisenberg chain calculated in reference [11a], for a coupling with site phonons, and in reference [11b], for a coupling with bond phonons. This shows also that $CuGeO_3$ is located in the vicinity of a quantum critical point (which could be reached under a modest negative pressure, as already emphasized in Ref. [12a]). In addition, as $\hbar\Omega_o \geq J$ there are important non-adiabatic corrections which renormalise J and introduce a next-near neighbour exchange interaction J' [45]. This could explain (at least partly) the unusual thermal dependence (with respect to the Bonner and Fischer behaviour expected for a $S = 1/2$ AF chain with only near-neighbour exchange interaction) of the spin susceptibility [38] of $CuGeO_3$, above T_{SP}.

$CuGeO_3$ exhibits a more pronounced quantum behaviour than the organic SP systems. MEM-$(TCNQ)_2$, with $\hbar\Omega_0 \sim \{\Delta_{MF}, J\}$, is in the gapped quantum region close to the boundary with the classical region [10,12]. Its spin susceptibility, which is not enough renormalised by the non-adiabatic corrections, still follows, above T_{SP}, the Bonner and Fischer thermal dependence of the $S = 1/2$ AF chain. $(TMTTF)_2X$ and $(BCPTTF)_2X$, with X = PF_6 and AsF_6, with $\hbar\Omega_0 < \{\Delta_{MF}, J\}$ belong to the classical region [10,12]. The SP fluctuations, which now occur in the adiabatic limit, lead to the formation of a pseudo-gap in the spin degrees of freedom which is accompanied by a drop of the spin susceptibility below T_{MF}, well above T_{SP} [14].

4.1.2 The Ni doped sample

According to our measurements, the pretransitional structural fluctuations of the Ni sample behave differently. Figure 7c shows that, in contrast with the other substituted samples and of pure $CuGeO_3$, ξ_b is larger than ξ_c, and that all the correlation lengths are quite short. ξ_a decreases extremely rapidly, so that the 3D-2D crossover temperature, T_{3D-2D}, occurs only 0.5 K above T_{SP}. 1 K above T_{SP}, ξ_c amounts to 6 Å (i.e. $c/2$) and ξ_b to 8 Å (i.e. b). In pure $CuGeO_3$, such short correlations are only observed at $T_{SP} + 16$ K and $T_{SP} + 4$ K, respectively (Fig. 3). The linear extrapolation of the thermal dependence of the inverse correlation length along b and c shows that, in the Ni sample, ξ_b^{-1} should reach $2/b$ at about $T_{SP} + 3$ K and that ξ_c^{-1} should reach $1/c$ at about $T_{SP} + 4$ K. Our measurements show that the pretransitional fluctuations of the Ni compound develop critically only a few K above T_{SP}, without the presence of a sizeable regime of 1D fluctuations. If this behavior is confirmed in other Ni samples and for other magnetic dopants such as Co, it would appear that the substitution of the Cu site by magnetic impurities kills the SP fluctuations of $CuGeO_3$. The finding that ξ_c is the most strongly reduced by the Ni substitution shows that the SP fluctuations are killed preferentially in chain direction. In this respect, it is interesting to note that the maximum of spin susceptibility, at about 55 K in pure $CuGeO_3$, has shifted drastically down to about 30K in the 0.9% Ni sample (see Fig. 1 in Ref. [36]). This could indicate that the 1D AF correlations are strongly reduced in the Ni samples, which consequence is to inhibit the SP structural fluctuations. A possible explanation for the reduction of the AF correlations could be that each $S = 1$ magnetic moment of the Ni impurity induces a ferromagnetic polarisation of the $S = 1/2$ Cu^{2+} located in its vicinity.

In this respect, magnetic impurities should perturb the magnetic chain differently from the non-magnetic impurities, such as Zn and Mg, whose effect is mainly to break the exchange path. In presence of non-magnetic impurities, the fragmentation of the AF chain does not disturb significantly the growth of the SP instability if the average distance between two neighbouring impurities in chain direction remains larger than the correlation length of the 1D AF fluctuations.

4.2 The structural disorder in the $CuGeO_3$ solid solutions

In this section we shall discuss the physical origin of the residual diffuse scattering observed in the alloys below T_{SP} (Fig. 8b and Ref. [17]). The non observation of a residual diffuse scattering in the SP phase of pure $CuGeO_3$ (Fig. 8a) means that the diffuse scattering is due to the X-ray scattering by parts of the sample where the spin-Peierls order is perturbed by the substituents. The general origin of such an X-ray scattering is explained in Section A.1 of the Annexe.

As the diffuse scattering basically corresponds to diffuse sheets in the reciprocal space, the perturbed regions have a pronounced 1D anisotropy in direct space. These perturbed regions mainly extend along the chain direction, c. In this direction, the width of the diffuse scattering does not vary significantly with the substituent and the concentration (at least for x and y smaller than 1%). These are evidences that the perturbed regions nucleated by all the substituents are basically similar, with a typical size of the order of $\xi_c^P = (\Delta Q_c)^{-1} \approx 25$ Å. In principle, the distribution function of the size of the perturbed domains could be obtained by a careful analysis of the profile of the diffuse scattering. This is considered in Section A.2 of the Annexe for domains in which the SP dimerisation is lost. In that case, the diffraction by a random distribution of

domain sizes gives a diffuse scattering with a Lorentzian profile (see expression (A.21)), while diffraction by a narrow distribution of domain size gives a diffuse scattering with a Gaussian-like profile (see expression (A.18)). Figure 4b shows that the shape of the diffuse scattering is closer to a Gaussian than to a Lorentzian. Thus, in the following we shall assume that all the perturbed regions keep the same shape and size whatever the substituent concentration. We consider in the Annexe different cases where the SP order is perturbed either by a loss of dimerisation (Sect. A.2) or by a dimerisation shifted by half a modulation period (Sect. A.3).

The perturbed regions are 1D for the Zn substituent on the Cu site of the magnetic chains. The perturbed region extends on a few neighbouring chains for the Si and Al substituents of the Ge atom which is located in-between the magnetic chains. The fact that interchain correlations along b depend upon the nature of the site which is substituted is another evidence that the diffuse scattering is induced by the dopant.

It is generally shown in the Annexe (Sect. A.1) that the X-ray scattering from a 3D SP array containing perturbed domains nucleated on the dopant positions, is the superimposition of a Bragg scattering term (whose peak intensity is reduced by the disorder — see expressions (A.13) and (A.22)) and of a diffuse scattering term whose profile, $G(k)$, is related to the Fourier transform of the form factor of the perturbed domain (see expressions (A.15) and (A.23)).

It has been observed that doping, through interrupting one or several chains, induces uncompensated $S = 1/2$ spins [20,22]. Theoretical considerations [23,24] have suggested that these spins develop AF correlations which extend on several Cu sites where the spin-Peierls order is destroyed or reduced. At low temperature, the dopant-induced magnetic domains couple antiferromagnetically [19,46]. Muon spin relaxation measurements of both Zn and Si doped materials [47] have shown that the AF order is spatially inhomogeneous with, if in each domain it is assumed that the moment size decays exponentially, a decay length of about $\xi_{AF} \sim 30$ Å in the chain direction. As ξ_{AF} is comparable to the domain size, $\xi_c^P \approx 25$ Å, where the SP order is perturbed in the doped materials, it is tempting to associate both kinds of perturbed regions.

For an isolated SP chain it is well-known [48,9a] that the excitation of lowest energy is a defect of dimerisation (or soliton). It extends over twice the SP coherence length ξ_{SP}. ξ_{SP}, the typical length on which the SP order can be destroyed, is given in the standard theory by:

$$\xi_{SP} = \hbar v_\sigma / \Delta, \tag{3}$$

where v_σ is the spin wave velocity and Δ is the SP (singlet-triplet) gap. In $CuGeO_3$, neutron scattering measurements [43,44] lead to $\hbar v_\sigma \approx 38$ meV Å and $\Delta \approx 2.4$ meV. Thus, one estimates $\xi_{SP} \approx 16$ Å. A defect of dimerisation consists of a non-paired spin, thus the soliton has an uncompensated spin 1/2. A periodic lattice of solitons can be generated by applying large magnetic fields, H, to a SP systems. In $CuGeO_3$, its structure has been accurately analysed both by structural [49,50] and magnetic [51,52] measurements. These studies give, for the structural counterpart of the soliton; an half width $\xi_{SP} \sim 40$ Å (which is 40% larger than the half width, $\sim\xi_{AF}$, of the magnetic counterpart of the soliton, a peculiar feature of $CuGeO_3$, due to frustrated J and J' AF couplings, and analyzed in Ref. [53]). This field induced ξ_{SP} value remains however substantially larger than the $H = 0$ value, $\xi_{SP} \sim 16$ Å, estimated by using expression (3).

It was suggested [23,24] that dopants can generate such $S = 1/2$ topological defects which, thus, will exhibit AF correlations over ξ_{SP}. In the 1D model developed in references [24–26], the dopant simply pins the soliton. However, the perturbation induced by the dopant in a 3D ordered SP lattice is more subtle because one has to take into account the change of phasing between the dimerisations located on neighbouring chains: a single soliton, which induces a shift of π in the phase of the dimerisation of the chain where it is located, changes also by π the phase of the dimerisation with respect to the dimers located on neighboring chains. This modifies the interchain coupling energy from a region of favorable coupling (where the neigbouring dimers are, let us say, out of phase) to a region of unfavorable coupling (where the neigbouring dimers are in phase). The unfavorable coupling energy can be minimized if a soliton is followed, on the same chain, by an antisoliton which restores the favorable interchain phasing. This realistic situation, which has been previously considered in references [23,28], is the basis of the interpretation of the experimental data obtained in a 3D ordered SP phase.

Figure 9 gives a schematical representation of the defect consisting of a soliton-antisoliton pair located respectively in $z = 0$ and $z = L_0$ in the chain direction. We shall consider it as the elementary pertubation of the 3D ordered array of SP dimers. For such a defect, the Cu displacement, $u(z)$, along the chain direction, $z = lc$, can be written:

$$u(z) = (-1)^l \, u_0[1 - f(z) + f(z - L_0)], \tag{4}$$

where the shape of the soliton is given by:

$$f(z) = \mathrm{th}(z/\xi_{SP}). \tag{5}$$

Figure 10a shows schematically how such a perturbed region can be nucleated on a spin neutral substituent of the Cu site. As a $S = 0$ site does not undergo the SP distortion, the soliton is pinned on the dopant position, and the antisoliton which restores the right interchain SP phasing is built with an unpaired Cu atom, located at L_0, which thus releases a spin $S = 1/2$. The formation of a bound state between the $S = 1/2$ and the nonmagnetic impurity has been obtained by numerical simulations taking explicitly into account the interchain elastic coupling energy between the SP distortions [28].

Figure 10b shows how the perturbed region can be nucleated on a substituent of the Ge site when the strain field (due to size or charge effects) associated with the dopant, forces the two first neighbouring Cu dimers closer to the

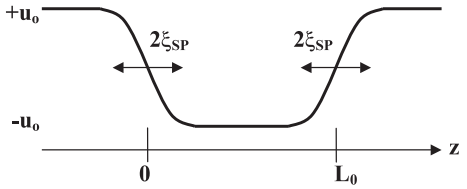

Fig. 9. Schematical representation of the defect of dimerisation made of a soliton-antisoliton pair.

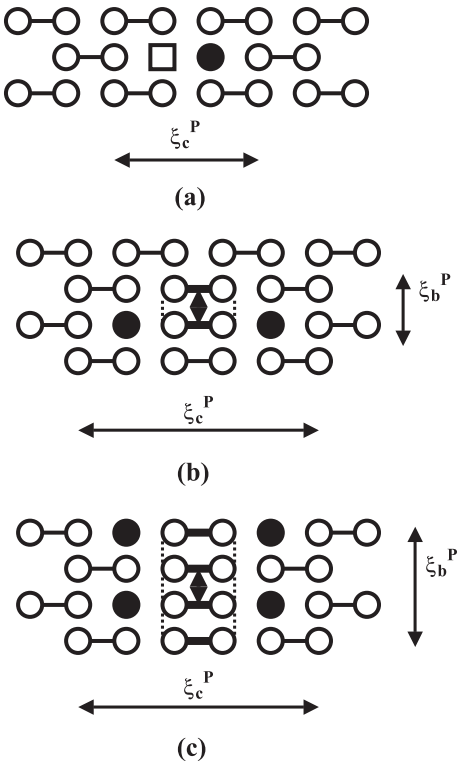

Fig. 10. Schematical representation of the 2D array of Cu^{2+} dimers (linked empty circles) perturbed by a non-magnetic substituent of the Cu site (empty squares) in (a), and by a substituent to the Ge site (full diamonds) which induces a strain field (dotted lines) on its neighbouring dimers in (b) and its next neighbouring dimers in (c). The unpaired Cu^{2+} are represented by full circles.

dopant to face each other. This process induces an uniform phasing between SP distortions on adjacent chains. This unfavorable lateral phasing can be disrupted by the formation of a soliton-antisoliton pair on one of these chains bound by the strain field. In such a case, two Cu atoms, separated by L_0, are not paired. This picture, where the non paired Cu are not located in the strict vicinity of the Si substituent, is in agreement with the NQR results of reference [65]. The defects of dimerisation shown in Figure 10b release two spins 1/2 per substituent. In the case of the Si dopant, there is an average of 3.3 spins 1/2 released per substituent [20]. Since the ionic radius difference between the Ge^{4+} and the Si^{4+} is quite large (see Tab. 1), it is thus possible that the strain field extends on second neighbouring chains. In such a case, shown Figure 10c, two soliton-antisoliton pairs, releasing four spins 1/2 per

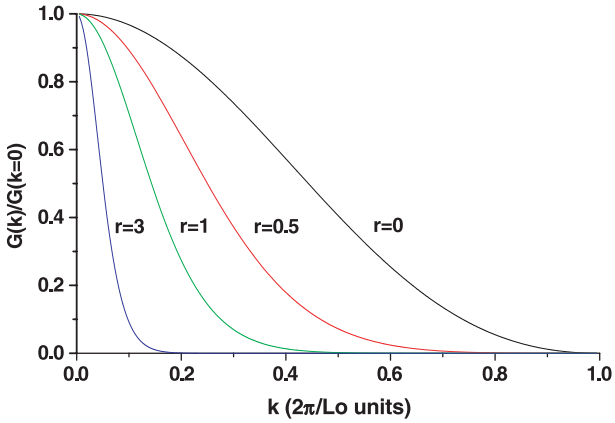

Fig. 11. k dependence of the normalized diffuse scattering term $G(k)/G(k=0)$ for different values of $r = \xi_{SP}/L_0$. $G(k)$ is given by the expression (6) and k is expressed in $2\pi/L_0 (= c^*/g_{k=0})$ units.

substituent, could be formed. The perturbation, which involves 3 neighbouring Cu chains on average, could be the superimposition of the situations shown Figures 10b and 10c.

It is shown in Section A.3 of the Annexe that, with a perturbation of the dimerisation described by expressions (4) and (5), the k dependence of the profile of the diffuse scattering is given in the chain direction by the expression (A.29):

$$G(k) = (\pi\xi_{SP}/c)^2[\sin(kL_0/2)/\mathrm{sh}(\pi k\xi_{SP}/2)]^2. \quad (6)$$

The shape of the profile depends upon the ratio $r = \xi_{SP}/L_0$. Typical profiles are shown in Figure 11. In principle a fit of the k dependence of the experimental profile by expression (6) should give L_0 and ξ_{SP}. However, in the present case, the intensity of the diffuse scattering is not strong enough to perform an accurate fit.

Below, we shall use the information given by the HWHM of the experimental diffuse scattering, ΔQ_c. For that purpose, Figure 12 gives the dependence of the reduced quantities $L_0\Delta Q$ and $\xi_{SP}\Delta Q$ as a function of r (for ≤ 3), in which ΔQ is the HWHM of the profiles calculated from expression (6). In the range of values shown, the r dependence of $L_0\Delta Q$ and $\xi_{SP}\Delta Q$ can be well accounted for by the analytical expression (A.32) of the Annexe, with an error less than 4% (continous lines in Fig. 12). However, from the single measurement of ΔQ_c, L_0 and ξ_{SP} cannot be obtained independently: one needs to know one length to obtain the other one. Below, we shall use three different methods to estimate one of these lengths, and we shall deduce the other one from the results of Figure 12.

4.2.1 Estimation of ξ_{SP}

Figure 12 shows that one always has $\xi_{SP}\Delta Q < 1$. Our measurements $\Delta Q_c = 0.04 \pm 0.005$ Å^{-1} gives thus an upper limit of 22−29 Å for ξ_{SP}. This limit is smaller than the half width, ∼40 Å, of the structural soliton lattice induced

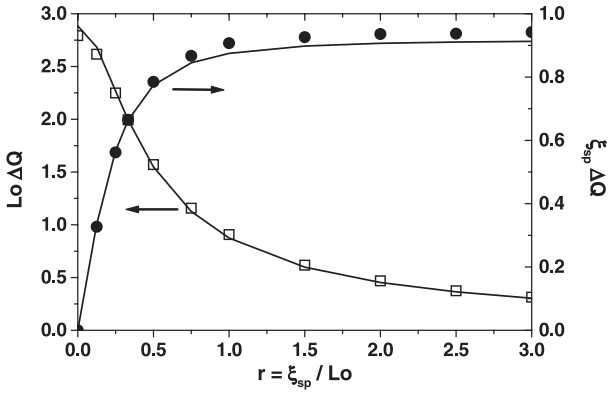

Fig. 12. Dependence of the reduced HWHM, $L_0\Delta Q$ (empty squares) and $\xi_{SP}\Delta Q$ (full circles), of the profile $G(k)$ shown Figure 11, as a function of the ratio $r = \xi_{SP}/L_0$. The continuous lines gives the reduced HWHM calculated by the expression (A.32).

under high magnetic field, H [49,50], which even increases when H decreases [51]. Thus, the data obtained from the magnetic field induced soliton lattice do not help getting a ξ_{SP} value consistent with the measurements performed at $H = 0$. We shall thus estimate ξ_{SP} by using the neutron data of references [43,44] in expression (3). This gives $\xi_{SP} = 16$ Å. With this value, the product $\xi_{SP}\Delta Q$ amounts to 0.55–0.72, and Figure 12 leads to $r \sim 0.25{-}0.4$, from which one deduces $L_0 \sim 40{-}64$ Å.

4.2.2 L_0 deduced from the decrease of the spin-Peierls satellite intensity

In presence of disorder, the intensity of the SP superlattice reflections is reduced firstly by the existence of perturbed regions where the amplitude of dimerisation vanishes (case considered in Sect. A.2 of the Annexe) and even changes of sign (case considered in Sect. A.3 of the Annexe and shown Fig. 9), and secondly by the (possible) decrease of the amplitude of dimerisation, $u_0(x)$, in the non-perturbed regions. In this case, the relative decrease of the satellite intensity, I_{SP}, is given, as a function of the dopant concentration x, by the expressions (A.13) or (A.22):

$$I_{SP}(x)/I_{SP}(0) = [f_P(x)\ u_0(x)/u_0(0)]^2, \tag{7}$$

where $f_P(x) = \langle g_n \rangle$ is the average amplitude of dimerisation normalized to the defect-free case ($f_P(0) = 1$). The relative variation of the amplitude of dimerisation can be related to the relative variation of the SP energy gap [41]:

$$u_0(x)/u_0(0) = [\Delta(x)/\Delta(0)]^{3/2}. \tag{8}$$

If one uses, for the Zn-doped samples, the neutron scattering data of reference [54], one gets:

- for the $x = 0.91\%$ sample: $u_0(x)/u_0(0) \approx 0.8$ from $\Delta(x)/\Delta(0) = 0.85$,
- for the $x = 0.74\%$ sample: $[I_{SP}(x)/I_{SP}(0)]^{1/2} = 0.6$.

This leads, for an average Zn concentration of 0.82%, to $f_P(\sim 0.8\%) = 0.75$.

With a perturbation of the amplitude of dimerisation described by the expressions (4) and (5), it is easy to show that g_n, averaged on the mean distance between two impurities c/x (assumed to be much larger than $2\xi_{SP}$) is given by expression (A.26):

$$f_P(x) = \langle g_n \rangle = 1 - 2xL_0/c. \tag{9a}$$

This leads, with $c = 2.94$Å, to $L_0 \sim 45$ Å.

If, within the framework of the calculation performed in Section A.2 of the Annexe, the dimerisation vanishes in the perturbed regions, one has instead of equation (9a):

$$f_P(x) = 1 - xL_0/c, \tag{9b}$$

which leads to $L_0 \sim 90$ Å.

If one uses the neutron scattering data of the Si-doped samples, one gets:

- for the $x = 0.7\%$ sample studied in reference [19]: $u_0(x)/u_0(0) \approx 0.6$ from $\Delta(x)/\Delta(0) = 0.71$,
- for the $x = 1\%$ sample studied in reference [55], which is more likely a 0.5% sample from its T_{SP} value: $[I_{SP}(x)/I_{SP}(0)]^{1/2} = 0.3$.

This leads, for an average Si concentration of 0.6%, to $f_P(\sim 0.6\%) = 0.50$. It is interesting to remark that this f_P value nearly amounts at the fraction, 0.35 ± 0.1, of Cu sites lost by NQR measurements (probably because of the presence of impurity-induced moments on these Cu sites) in the 0.6% Si sample recently investigated in reference [65] (see in particular Fig. 2b in this reference).

By considering that the defect involves $n_b = 3$ chains, expression (9a) becomes:

$$f_P(x) = 1 - 2xn_bL_0/c, \tag{10a}$$

which gives $L_0 \sim 40$ Å, and expression (9b) becomes:

$$f_P(x) = 1 - xn_bL_0/c, \tag{10b}$$

which gives $L_0 \sim 80$ Å.

In the case where the dimerisation vanishes in the perturbed region, L_0 values are twice larger than L_0 obtained for a perturbed region consisting of a phase shift of the dimerisation by half a repeat period. The L_0 values obtained in the latter case agree quite well with those estimated in Section 1. Thus, in the following, we shall consider that the model of Section A.3 of the Annexe is the best.

With an average value $L_0 = 42.5$ Å one gets: $L_0\Delta Q \sim 1.5{-}1.9$. From Figure 11, one obtains $r \sim 0.38{-}0.55$. This leads to $\xi_{SP} \sim 16{-}23$ Å, a range of values which overlaps ξ_{SP} determined in Section 1.

In expression (7) we have neglected a possible enhancement with x of the Debye-Waller factor of the SP reflections due to disorder induced spatial variations of the dimerisation amplitude. However, we do not believe that this effect could change significantly the results because u_0 is very small and the superlattice intensity has been

measured for SP reflections located at small Q reciprocal positions where the corrections of the Debye Waller factor are the smallest.

The 1D model developed in references [24–26] predicts, with x, a drop of the SP satellite intensity much smaller than the one experimentally observed. We think that the reason of the discrepancy of the 1D model (where each dopant induces only a soliton of size $2\xi_{SP}$) with the experimental results is that in the true (i.e. 3D) SP phase each dopant induces a soliton-antisoliton pair, separated by L_0, where the amplitude of dimerisation is reduced or even changes of sign.

4.2.3 L_0 deduced from the drop of T_{SP}

Several authors have already shown that the formation of dopant-induced solitons is responsible for the drop of the critical temperature, T_{SP}, of the long range SP order [23]. Here we shall present a very simple calculation which accounts quite well for the experimental rate of decrease of T_{SP}. It relies on the key role played by the interchain coupling to achieve a 3D order, in a system dominated by 1D fluctuations. The basic ingredient of the calculation is that if the interchain coupling between dimerised regions (i.e. between first neighbouring sites along b) fixes the T_{SP} value, the presence of non-dimerised domains (or dimerised domains with the wrong phasing) will diminish the coupling energy, and thus T_{SP}. If -2σ is the gain of interchain coupling energy per dimerised site when each site is surrounded by two dimerised chains (along b) with a π phasing, the energy lost by a dimerised site which has the wrong (i.e. zero) phasing with its neighbouring dimers is $+2\sigma$. If a perturbed domain contains n_b chains with the wrong phasing, which each extends on L_0/c sites, the energy lost, with respect to the ground state energy of -2σ per site, is: $2(n_b+1)\sigma L_0/c$ per site. If the relative decrease of T_{SP} is proportional to the average loss of interchain coupling energy per site, one simply gets, for a concentration $1/x$ of domain:

$$[T_{SP}(0) - T_{SP}(x)]/T_{SP}(0) = x(n_b+1)L_0/c, \qquad (11)$$

and thus:

$$d\ln[T_{SP}(x)]/dx = -(n_b+1)L_0/c. \qquad (12)$$

In the case of the Zn-doped samples, with $n_b = 1$, the decrease rate:

$$dT_{SP}(x)/dx \approx -2.1 \text{ K/\%},$$

obtained by the magnetic measurements of reference [22] (see also Tab. 2), leads to $L_0 \approx 22$ Å.

In the case of the Si doped samples, with $n_b = 3$, and with the decrease rate:

$$dT_{SP}(x)/dx \approx -6.3 \text{ K/\%},$$

obtained by the magnetic measurements in reference [20], one gets $L_0 \approx 32$ Å.

In the case of the Al sample, with $n_b = 2$, and with the decrease rate:

$$dT_{SP}(x)/dx \approx -4.2 \text{ K/\%},$$

determined Table 2, one obtains $L_0 \approx 29$ Å.

With an average value $L_0 = 28$ Å, slightly smaller than the L_0 value determined in Sections 1 and 2, one gets: $L_0\Delta Q \sim 1{-}1.25$. From Figure 11, one obtains $r \sim 0.7{-}0.9$. This leads to $\xi_{SP} \sim 20{-}25$ Å, which is slightly larger than the ξ_{SP} value determined in Section 1, but which contains the ξ_{SP} values of Section 2.

4.2.4 Summary of the results

In summary, there is a general overall agreement between the three independent determinations of ξ_{SP} and L_0, assuming a model (shown Fig. 9) where, in the perturbed regions, the dimerisation shifts by half a repeat period. Reasonable values of ξ_{SP} are in the range 16–20 Å, and those of L_0 are in range 28–45 Å. With these values, one roughly has: $L_0 \sim 2\xi_{SP}$. This corresponds to $r \sim 0.5$, for which expression (6) gives a profile close to a Gaussian and which accounts quite well for the experimental profile shown in Figure 4b for the 0.1% Si sample.

For $r \sim 0.5$, the soliton and the antisoliton limiting the perturbed domain begin to overlap. This situation corresponds to that found in the numerical simulations of reference [28]. It shows that the interchain coupling is strong enough to prevent the sizeable development of the dimerisation with the wrong interchain phasing.

These determinations allow to estimate that the overall size of the perturbated domain amounts at about:

$$L = L_0 + 2\xi_{SP} \sim 70 \text{ Å}.$$

In the case where the soliton and the antisoliton, bearing the AF correlations, begin to overlap it appears that L is also comparable to the typical size of the magnetic domains. Consistently, L amounts to the size ($2\xi_{AF} \sim 60$ Å) of the magnetic inhomogeneities determined by muon spin relaxation in the AF phase of doped $CuGeO_3$ [47].

With these data, one can also estimate the critical concentration, x_c, above which the long range SP order is destroyed. Basically, the long range SP order will disappear: (i) transversally if, on adjacent chains, there is no dimerised segments with the correct phasing which overlap each other and (ii) longitudinally if, on a given chain, two dimerised segments interrupted by a defect, do not overlap with a dimerised segment having the correct phasing on a neighbouring chain. Crudely, the long range SP order will vanish if the average length of a non-perturbed domain becomes less than the size, L, of a perturbed domain. This gives, for a substituent of the Cu site:

$$(c/x) - L < L, \qquad (13)$$

or:

$$x > x_c \approx c/2L. \qquad (14)$$

With $L \sim 70$ Å, one gets $x_c \sim 2.1\%$. This critical concentration surprisingly corresponds to the critical value of $x_c \sim 2.1\%$ determined by structural measurements in the Mg-doped samples [34] and of $x_c \sim 2.2\%$ estimated from magnetic measurements in the Zn-doped samples [22]. In the case of a substituent of the Ge site, where the perturbed domain involves n_b chains, one gets:

$$x_c \approx c/2n_bL.$$

For the Si-doped samples, with $n_b = 3$, one obtains $x_c \sim 0.7\%$. This critical concentration is very close to the critical value $x_c \sim 0.8\%$ estimated from magnetic measurements in the Si-doped samples [20].

For x larger than x_c, the SP order will persist under the form of a short range order. Indeed, diffraction by the longitudinal short range SP order has been detected for higher dopant concentration (1.5% and 5%) in the Si-doped samples [56].

4.3 Comparison with the other disordered spin-Peierls systems

The observation (for $x < x_c$) of a long range SP order in doped $CuGeO_3$ is not surprising since it is established [57] on theoretical grounds that the dimerized spin-1/2 chain is stable against disorder. However, to our knowledge, this is the first time that such a feature is really observed. The long range order is rapidly destroyed by the defects in the other SP systems (mostly the organic 2:1 cation or anion radical organic charge transfer salts). We believe that the reason is that the substitutional disorder in $CuGeO_3$ preserves the long range array of localised charges (i.e. the crystallographic structure of the Cu^{2+} lattice which bears the spins $1/2$), while in the 2 : 1 organic salts the disorder limits primarily the correlation length, ξ_{4k_F}, of the lattice of localised charges (i.e. of the $4k_F$ charge density wave). Since in the soft 1D organic salts there is one charge every two molecules, the $4k_F$ lattice of localised charges is accompanied by a dimerisation of the stack. In presence of disorder there is a short-range dimerisation and, thus, short-range charge localization. In that situation if, below the spin-charge decoupling temperature (T_ρ), SP correlations develop between the localized spins $1/2$, its correlation length will be capped by ξ_{4k_F}. As generally in quasi-1D conductors, ξ_{4k_F} decreases rapidly with the amount of disorder, the long range SP order (which consists in a tetramerisation of the organic stack) will be rapidly destroyed. This is what is observed in 2 : 1 TCNQ salts such as $Qn(TCNQ)_2$ and the solid solution $NMP_xPhen_{1-x}TCNQ$ for $x \sim 0.5$. In these salts, a quasi-1D charge localization is observed on a ξ_{4k_F} of a few 10 Å and, below T_ρ, a quasi-1D SP local distortion takes place on about the same correlation length [58,59]. At low temperature, these 1D salts can be viewed as consisting of AF chains interrupted by non-magnetic segments where a local SP distortion takes place. Their spin susceptibility, which follows a low temperature $T^{-\alpha}$ divergence, is indicative of a quantum disordered phase (see for example [60]).

A situation somewhat symmetric to that observed in disordered $CuGeO_3$, which basically exhibits 1D AF segments in a 3D SP phase, can be found in the organic salt $(TMDTDSF)_2PF_6$ which presents 1D short range SP order in a 3D AF phase [61]. This salt exhibits an orientational disorder of the non-centrosymmetrical TMDTDSF molecule, which is an hybrid between the Se based (TMTSF) and the S based (TMTTF) molecules [62]. At the difference of the point disorder of $CuGeO_3$, which basically perturbs locally the exchange path, the random orientational disorder of $(TMDTDSF)_2PF_6$ induces a distribution of exchange integrals. In the presence of this kind of disorder, the AF ground state is probably stabilized by the interchain coupling as in disordered $CuGeO_3$ [60]. The 1D SP segments observed in the $(TMDTDSF)_2PF_6$ hybrid salt are the remaining trace of the SP order which develops in $(TMTTF)_2PF_6$ (the SP order is probably nucleated in the parts of the TMDTDSF organic stacks where, because of the random orientational disorder, the S atoms of the molecules face each other).

5 Conclusion

In this paper we have confirmed that the SP transition of $CuGeO_3$ is announced by a sizeable regime of 1D pretransitional fluctuations taking place along the chain direction c. We have shown that the crossover temperature to the regime of 2D fluctuations, in the bc plane, occurs only 10 K above T_{SP}. The transition to a 3D long range SP order occurs at a T_{SP} corresponding to $1/4$ of the temperature of preformation of singlet dimers (T_{MF}), that we estimate at about 50 K. For a low amount of dopant, the 3D SP order remains of long-range type, as previously found, and the pretransitional fluctuations remain critical. The anisotropy and the thermal dependence of these fluctuations are not significantly modified by the presence of non-magnetic substituents of the Cu site or of the Ge site. This is not the case for a magnetic substituent, such as Ni, of the Cu site.

Our X-ray diffuse scattering investigation shows that the SP ground state of doped samples contains quasi-1D defects. We have modelized the disorder in doped $CuGeO_3$ by the formation of soliton-antisoliton pairs, in the magnetic chain direction, which are pinned either to the substituent of the Cu site or to the deformation field induced by the substituent of the Ge site. We have estimated the impurity-induced soliton half width ξ_{SP} at about 16–20 Å, a value which is two times smaller than ξ_{SP} of the magnetic field-induced soliton lattice of $CuGeO_3$, and that the separation between the soliton and the antisoliton, L_0, amounts at about 28–45 Å. With these numbers, we are able to quantitatively account for the drop of T_{SP} as a function of the dopant concentration, and to estimate the critical concentration x_c above which the long range SP order vanishes. The overall size of the perturbed domains, $L_0 + 2\xi_{SP} \sim 70$ Å, thus obtained is comparable with the size of the magnetic inhomogeneities determined by muon spin spectroscopy in the AF phase of doped $CuGeO_3$.

D. Petermann is thanked for his help during the analysis of the data.

Annexe

The purpose of this annexe is to calculate the X-ray scattering from an inhomogeneous (i.e. doped) crystal which has undergone a long range (SP) structural modulation and which contains domains where the modulation is perturbed. In Section A.1, we shall recall some general diffraction expressions for a toy model of a crystal containing atomic vacancies. We shall apply these expressions in Section A.2 for a SP modulation with vacancies of dimerisation, and, in Section A.3, for a SP modulation containing domains where the phase of the dimerisation jumps of π because of the formation of soliton-antisoliton pairs.

A.1 Diffraction by a crystal with atomic vacancies

Let us consider a crystal of volume V with N sites of coordinate $\mathbf{r}_n$. This crystal contains $M < N$ atoms of form factor f, and thus $N - M$ atomic vacancies. The amplitude diffracted by the crystal is simply:

$$A(\mathbf{q}) = \sum_n \sigma_n f \exp(-i\mathbf{q}\mathbf{r}_n), \tag{A.1}$$

with $\sigma_n = 1$ if the site $\mathbf{r}_n$ is occupied by an atom, $\sigma_n = 0$ otherwise. $x = \langle\sigma_n\rangle = M/N$ is the fraction of the sites occupied. In this toy model the long-range order is due to a periodic lattice of sites which is preserved even in presence of atomic vacancies.

The X-ray intensity scattered by this crystal is given by:

$$I(\mathbf{q}) = |A(\mathbf{q})|^2. \tag{A.2}$$

$I(\mathbf{q})$ is the sum of a Bragg reflection term and of a diffuse scattering term (schematically shown Fig. 13b). The intensity of the Bragg reflections is given by:

$$I_B(\mathbf{q}) = (xf)^2 \sum_{h,k,l} \delta(\mathbf{q} - \mathbf{Q}_{h,k,l}), \tag{A.3}$$

where $\mathbf{Q}_{h,k,l}$ is a reciprocal wave vector of the lattice of sites.

The diffuse scattering term is given by:

$$\begin{aligned} I_D(\mathbf{q}) &= f^2 \sum_m \langle(\sigma_n - x)(\sigma_{n+m} - x)\rangle_n \exp(-i\mathbf{q}\mathbf{r}_m) \\ &= f^2 \sum_m G(m) \exp -(i\mathbf{q}\mathbf{r}_m), \end{aligned} \tag{A.4}$$

where $\langle....\rangle_n$ means a spatial average, and $G(m)$ is the vacancy correlation function. If one introduces σ_k, the Fourier transform of $\sigma_n - x$:

$$\sigma_n - x = (N)^{-1/2} \sum_k \sigma_k \exp(-i\mathbf{k}\ \mathbf{r}_n), \tag{A.5}$$

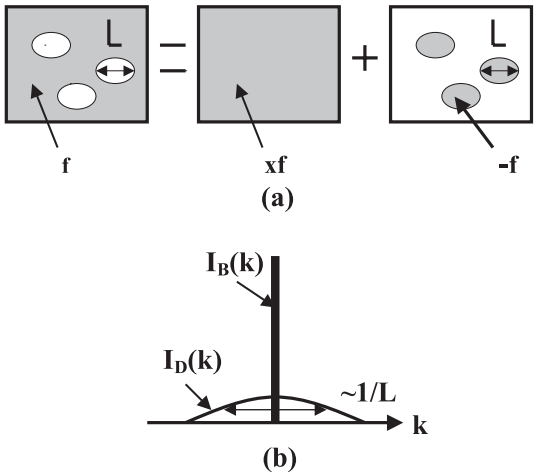

Fig. 13. (a) Decomposition of the diffraction process in an inhomogeneous long-range ordered periodic medium (containing uncorrelated domains with atomic vacancies) into the sum of the diffraction from a homogeneous long range ordered periodic medium (with atoms of effective form factor xf) and of the diffraction from a collection of independent diffracting domains (with "anti-atoms" of form factor $-f$). (b) Schematical representation of the diffraction pattern from such a medium consisting of the sum of a Bragg reflection term, $I_B(q)$, and of a diffuse scattering term $I_D(q)$.

expression (A.4) becomes:

$$I_D(\mathbf{q} = \mathbf{Q}_{h,k,l} + \mathbf{k}) = f^2|\sigma_k|^2. \tag{A.6}$$

If there is a random distribution of vacancies, one recovers the ($\mathbf{k}$ independent) Laüe scattering term:

$$I_D(\mathbf{q}) = Nf^2x(1-x). \tag{A.7}$$

If there are correlation between the vacancies, $I_D(\mathbf{q})$ gives a $\mathbf{k}$ dependent diffuse scattering term centered on each Bragg reflection and whose $\mathbf{k}$ dependence is given by $G(\mathbf{k}) = |\sigma_k|^2$, which corresponds to the Fourier transform of $G(m)$.

As shown in Figure 13a, $I(\mathbf{q})$ corresponds at the sum of the scattering by an homogeneous periodic crystal, where all the sites are occupied by an effective atom of form factor xf (entering in the expression (A.3)), and of the scattering by "anti-atoms", of form factor $-f$, located in domains which Fourier transform of the form factor is given by $|\sigma_k|^2$.

It is interesting to calculate the integrated intensity of these two different terms over a Brillouin zone (of volume $1/v = (2\pi)^3 N/V$):

$$\int_{BZ} I_B(\mathbf{q}) d^3\mathbf{q} = x^2 f^2 N/v \tag{A.8}$$

$$\int_{BZ} I_D(\mathbf{q}) d^3\mathbf{q} = x(1-x) f^2 N/v. \tag{A.9}$$

The integrated total intensity amounts to:

$$\int_{BZ} I(\mathbf{q}) d^3\mathbf{q} = xf^2 N/v = Mf^2/v. \tag{A.10}$$

As expected, only this last quantity is proportional to the total number $M = xN$ of atoms.

A.2 Spin-Peierls crystal with dimerisation vacancies

We generalize the expressions of Section A.1 by assuming that the long-range SP phase (of amplitude of dimerisation u, and of modulation wave vector $\mathbf{q}_{SP}$ such that $\exp i\mathbf{q}_{SP}\mathbf{r}_n = (-1)^n$) contains sites which do not undergo the dimerisation. By defining the variable σ_n as in Section A.1, the amplitude diffracted by the modulated crystal is:

$$A(\mathbf{q}) = \sum_n f \exp[-i\mathbf{q}(\mathbf{r}_n + \sigma_n(-1)^n\mathbf{u})]. \quad (A.11)$$

If $\mathbf{qu} \ll 1$, expression (A.11) becomes:

$$A(\mathbf{q}) = \sum_n f \exp(-i\mathbf{q}\mathbf{r}_n)[1 + \sigma_n(-1)^n\mathbf{qu})]. \quad (A.12)$$

In addition to the main Bragg reflections, the dimerisation now induces superlattice reflections located in $\mathbf{Q}_{h,k,l}+\mathbf{q}_{SP}$ and of intensity:

$$I_{SP}(\mathbf{q}) = (xf\mathbf{qu})^2 \sum_{h,k,l} \delta(\mathbf{q} - \mathbf{Q}_{h,k,l} - \mathbf{q}_{SP}). \quad (A.13)$$

This generalizes the expression (A.3), with $x = \langle\sigma_n\rangle$ being the fraction of non modulated sites.

The diffuse scattering term given by expression (A.4) is generalized by:

$$I_D(\mathbf{q}) = (f\mathbf{qu})^2 \sum_m (-1)^m G(m) \exp(-i\mathbf{q}\mathbf{r}_m), \quad (A.14)$$

with $G(m) = \langle(\sigma_n - x)(\sigma_{n+m} - x)\rangle_n$. Expression (B.4) becomes:

$$I_D(\mathbf{q} = \mathbf{Q}_{h,k,l} + \mathbf{q}_{SP} + \mathbf{k}) = |f\mathbf{qu}|^2|\sigma_k|^2. \quad (A.15)$$

The integrated intensities follow the same relationships as those given by expressions (A.8–A.10), with $f \to f\mathbf{qu}$.

In $CuGeO_3$ $I_D(\mathbf{q})$ has the anisotropy of a diffuse sheet. This corresponds to the Fourier transform of a 1D correlation function $G(m)$ in direct space.

If the domains of vacancies have all the same size L_0, one has [63]:

$$\begin{aligned} G_0(m) &= 1 - |m|c/L_0 \quad \text{for} \quad |m|c < L_0, \\ G_0(m) &= 0 \quad\quad\quad\quad\ \text{for} \quad |m|c > L_0. \end{aligned} \quad (A.16)$$

From which one gets:

$$G_0(k, L_0) = [\sin(kL_0/2)/(kc/2)]^2. \quad (A.17)$$

If now there is a narrow distribution of domain sizes, around the mean value $L_0(\gg\sigma)$, described by the gaussian probability:

$$P_\sigma(L - L_0) = \left(\sqrt{2}\pi\sigma\right)^{-1} \exp[-(L - L_0)^2/2\sigma^2],$$

one gets:

$$\begin{aligned} G_\sigma(k, L_0) &= G_0(k, L) * P_\sigma(L - L_0) \\ &= G_0(k, L_0)\exp(-k^2\sigma^2/2) + o(k^2\sigma^4/c^2), \end{aligned} \quad (A.18)$$

whose k dependence is close to a Gaussian.

If there is a random distribution of domain sizes [64], and if μ is the linear probability to cross, per unit length, a domain wall which limits the vacancy region, one has:

$$G_\mu(m + dm) = G_\mu(m)[1 - \mu cdm]. \quad (A.19)$$

The solution of this differential equation is:

$$G_\mu(m) = \exp(-\mu cm) \quad (A.20)$$

whose 1D Fourier transform is a Lorentzian:

$$G_\mu(k) \propto 1/c^2[\mu^2 + k^2]. \quad (A.21)$$

A.3 Spin-Peierls crystal with domains where the amplitude of dimerisation varies

In that case one can write the amplitude of dimerisation in these domains under the form $g_n\mathbf{u}$. g_n plays the same role as σ_n in Section A.2. Expression (A.13) becomes:

$$I_{SP}(\mathbf{q}) = (f\mathbf{qu}\langle g_n\rangle)^2 \sum_{h,k,l} \delta(\mathbf{q} - \mathbf{Q}_{h,k,l} - \mathbf{q}_{SP}), \quad (A.22)$$

and expression (A.15) becomes:

$$I_D(\mathbf{q} = \mathbf{Q}_{h,k,l} + \mathbf{q}_{SP} + \mathbf{k}) = |f\mathbf{qu}|^2|g_k|^2, \quad (A.23)$$

with:

$$g_k = (N)^{-1/2} \sum_k (g_n - \langle g_n\rangle) \exp(i\mathbf{k}\ \mathbf{r}_n). \quad (A.24)$$

If one takes the expressions (4) and (5) to describe the perturbation of modulation shown Figure 9, one has:

$$g_n = [1 - f(nc) + f(nc - L_0)], \quad (A.25)$$

with:

$$f(nc) = \mathrm{th}(nc/\xi_{SP}).$$

It is easy to show that g_n averaged on the distance, c/x, between two substituents (assumed to be larger than $2\xi_{SP}$) is:

$$\langle g_n\rangle \approx 1 - 2xL_0/c. \quad (A.26)$$

If $L_0 \ll c/x$ one has:

$$g_n - \langle g_n\rangle \approx f(nc - L_0) - f(nc), \quad (A.27)$$

whose Fourier transform is:

$$g_k = (\pi\xi_{SP}/c)[\sin(kL_0/2)/\mathrm{sh}(\pi k\xi_{SP}/2)]. \quad (A.28)$$

The limit $k = 0$ is such that:

$$g_{k=0} = L_0/c$$

gives the number of sites limited by a soliton-antisoliton pair.

From (A.28), one gets:

$$G(k) = |g_k|^2 = (\pi\xi_{SP}/c)^2[\sin(kL_0/2)/\mathrm{sh}(\pi k\xi_{SP}/2)]^2, \quad \text{(A.29)}$$

whose k dependence is governed by the ratio $r = \xi_{SP}/L_0$. Typical profiles are shown Figure 11.

For $r = 0$, the profile has a:

$$G(k) = [\sin(kL_0/2)/(kc/2)]^2 \quad \text{(A.30)}$$

dependence (also given by (A.17)). One has $L_0 = 0.888\pi\xi_c^P$, and where ξ_c^P is the inverse of the HWHM of the diffuse scattering, ΔQ_c. $G(k)$ given by (A.30) vanishes for $k = 2\pi p/L_0$, and exhibits secondary maxima for $k = 2\pi(p + 3/2)/L_0$, where p is an integer. The intensity of these maxima decreases when p increases. The intensity of the first one ($p = 1$) is only 4.5% of $G(k = 0)$. The secondary maxima vanish exponentially when r increases.

When r increases, the k dependence of $G(k)$ also evolves towards that of a Gaussian. Figure 11 shows that $G(k)$ is very close to a Gaussian for $r \sim 0.5$.

Expression (A.29) becomes, for q small:

$$G(k) \approx (L_0/c)^2 \exp -(k\xi_G)^2, \quad \text{(A.31)}$$

with:

$$\xi_G^2 = \left(L_0^2 + \pi^2\xi_{SP}^2\right)/12 \approx \ln 2(\xi_c^P)^2. \quad \text{(A.32)}$$

When r increases further, the k dependence of $G(k)$ evolves towards that of a Lorentzian square. The Lorentzian square profile is only reached in the limit $r \gg 1$. In that case $G(k)$ becomes:

$$G(k) = (L_0/c)^2/\left[1 + (k\xi_L)^2\right]^2, \quad \text{(A.33)}$$

with $\xi_L = \pi\xi_{SP}/2\sqrt{6}$, or $\xi_{SP} \approx \xi_c^P$.

References

1. Special issue on "Electronic Cooperation", Science **288**, 461–482 (2000)
2. A.J. Millis, Physica B **312–313**, 1 (2002)
3. S.M. Girvin, Solid State Commun. **107**, 623 (1998)
4. T.M. Rice, in *High Magnetic Fields: Applications in Condensed matter Physics and Spectroscopy*, edited by C. Berthier, L.P. Lévy, G. Martinez, Lecture Notes in Physics **595** (Springer, 2001), p. 139; E. Dagotto, T.M. Rice, Science **271**, 618 (1996)
5. See for example, H. Fukuyama, Synth. Met. **19**, 63 (1987)
6. K. Nomura, K. Okamoto, J. Phys. A **27**, 5773 (1994)
7. P.W. Anderson, Mater. Res. Bull. **8**, 153 (1973)
8. See for example, H. Fukuyama, M. Saito, J. Phys. Soc. Jpn **69**, suppl. B, 122 (2000)
9. (a) T. Nakano, H. Fukuyama, J. Phys. Soc. Jpn **49**, 1679 (1980); T. Nakano, H. Fukuyama, J. Phys. Soc. Jpn **50**, 2489 (1981); (b) A.I. Buzdin, M.L. Kulic, V.V. Tugushev, Solid State Commun. **48**, 483 (1983); (c) M. Fujita, K. Machida, J. Phys. C **21**, 5813 (1988)
10. L.G. Caron, S. Moukouri, Phys. Rev. Lett. **76**, 4050 (1996)
11. (a) R.J. Bursill, R.H. McKenzie, C.J. Hamer, Phys. Rev. Lett. **83**, 408 (1999); in this paper the g couplig corresponds to $\alpha/2$ in our notations; (b) D. Augier, thesis, University of Toulouse, France, 1999 (see Figure II.24 in particular)
12. (a) J.P. Pouget, Eur. Phys. J. B **20**, 321 (2001); (b) Erratum, Eur. Phys. J. B **24**, 415 (2001) (with the definition of Δ used in the erratum the right member of its expression (3) must be multiplied by 2)
13. Q. Liu, S. Ravy, J.P. Pouget, C. Coulon, C. Bourbonnais, Synth. Met. **55–57**, 1840 (1993)
14. B. Dumoulin, C. Bourbonnais, S. Ravy, J.P. Pouget, C. Coulon, Phys. Rev. Lett. **76**, 1360 (1996)
15. G.S. Uhrig, Physica B **280**, 308 (2000)
16. J.P. Pouget, L.P. Regnault, M. Ain, B. Hennion, J.P. Renard, P. Veillet, G. Dhalenne, A. Revcolevschi, Phys. Rev. Lett. **72**, 4037 (1994)
17. J.P. Schoeffel, J.P. Pouget, G. Dhalenne, A. Revcolevschi, Phys. Rev. B **53**, 14971 (1996)
18. S. Ravy, J.P. Pouget, S. Grenier, A. Troader, J.E. Lorenzo, Y. Joly, H. Renevier, B. Grenier, J.Y. Henry, L.P. Regnault, J. Jegoudez, G. Dhalenne, A. Revcolevschi, in *Quantum Properties of Low-Dimensional Antiferromagnets*, edited by Y. Ajiro, J.P. Boucher (Kyushu University Press, 2002), p. 151
19. L.P. Regnault, J.P. Renard, G. Dhalenne, A. Revcolevschi, Europhys. Lett. **32**, 579 (1995)
20. B. Grenier, J.P. Renard, P. Veillet, C. Paulsen, R. Calemczuk, G. Dhalenne, A. Revcolevschi, Phys. Rev. B **57**, 3444 (1998)
21. T. Masuda, A. Fujioka, Y. Uchiyama, I. Tsukada, K. Uchinokura, Phys. Rev. Lett. **80**, 4566 (1998)
22. B. Grenier, J.P. Renard, P. Veillet, C. Paulsen, R. Calemczuk, G. Dhalenne, A. Revcolevschi, Phys. Rev. B **58**, 8202 (1998)
23. D. Khomskii, W. Geertsma, M. Mostovoy, Czech. J. Phys. **46**, suppl. S6, 3229 (1996); M. Mostovoy, D. Khomskii, Z. Phys. B **103**, 209 (1997)
24. H. Fukuyama, T. Tanimoto, M. Saito, J. Phys. Soc. Jpn **65**, 1182 (1996)
25. M. Saito, H. Fukuyama, J. Phys. Soc. Jpn **66**, 3259 (1997)
26. M. Saito, J. Phys. Soc. Jpn **67**, 2477 (1998)
27. M. Fabrizio, R. Mélin, J. Souletie, Eur. Phys. J. B **10**, 607 (1999)
28. P. Hansen, D. Augier, J. Riera, D. Poiblanc, Phys. Rev. B **59**, 13557 (1999)
29. A. Revcolevschi, R. Collongues, C. R. Acad. Sci. Paris **266**, 1767 (1969)
30. G. Dhalenne, A. Revcolevschi, J.C. Rouchaud, M. Fedoroff, Mater. Res. Bull. **32**, 939 (1997)
31. K. Hirota, D.E. Cox, J.E. Lorenzo, G. Shirane, J.M. Tranquada, M. Hase, K. Uchinokura, H. Kojima, Y. Shibuya, I. Tanaka, Phys. Rev. Lett. **73**, 736 (1994)
32. J.E. Lorenzo, L.P. Regnault, S. Langridge, C. Vettier, C. Sutter, G. Grübel, J. Souletie, J.G. Lussier, J.P. Schoeffel, J.P. Pouget, A. Stunault, D. Wremeille, G. Dhalenne, A. Revcolevschi, Europhys. Lett. **45**, 45 (1999)

33. Y.J. Wang, Y.-J. Kim, R.J. Christianson, S.C. LaMarra, F.C. Chou, R.J. Birgeneau, Phys. Rev. B **63**, 052502 (2001)
34. Y.J. Wang, V. Kiryukhin, R.J. Birgeneau, T. Masuda, I. Tsukada, K. Uchinokura, Phys. Rev. Lett. **83**, 1676 (1999)
35. M. Hase, I. Terasaki, Y. Sasago, K. Uchinokura, H. Obara, Phys. Rev. Lett. **71**, 4059 (1993)
36. B. Grenier, A.-L. Barra, P. Monod, S. Clément, J.-P. Renard, G. Dhalenne, A. Revcolevschi, Physica B **259–261**, 961 (1999)
37. M. Weiden, W. Richter, C. Geibel, F. Steglich, P. Lemmens, B. Eisener, M. Brinkmann, G. Güntherodt, Physica B **225**, 177 (1996)
38. K. Fabricius, A. Klûmper, U. Löw, B. Büchner, T. Lorenz, G. Dhalenne, A. Revcolevschi, Phys. Rev. B **57**, 1102 (1998)
39. P.H.M. van Loosdrecht, J.P. Boucher, G. Martinez, G. Dhalenne, A. Revcolevschi, Phys. Rev. Lett. **76**, 311 (1996)
40. H. Winkelmann, E. Gamper, B. Büchner, M. Braden, A. Revcolevschi, G. Dhalenne, Phys. Rev. B **51**, 12884 (1995)
41. M.C. Cross, D.S. Fisher, Phys. Rev. B **19**, 402 (1979)
42. M. Braden, B. Hennion, W. Reichardt, G. Dhalenne, A. Revcolevschi, Phys. Rev. Lett. **80**, 3634 (1998)
43. M. Nishi, O. Fujita, J. Akimitsu, Phys. Rev. B **50**, 6508 (1994)
44. L.P. Regnault, M. Ain, B. Hennion, G. Dhalenne, A. Revcolevschi, Phys. Rev. B **53**, 5579 (1996)
45. G.S. Uhrig, Phys. Rev. B **57**, R14004 (1998)
46. J.P. Renard, K. Le Dang, P. Veillet, G. Dhalenne, A. Revcolevschi, L.P. Regnault, Europhys. Lett. **30**, 475 (1995)
47. K.M. Kojima, Y. Fudamoto, M. Larkin, G.M. Luke, J. Merrin, B. Nachumi, Y.J. Uemura, M. Hase, Y. Sasago, K. Uchinokura, Y. Ajiro, A. Revcolevschi, J.P. Renard, Phys. Rev. Lett. **79**, 503 (1997)
48. M. Grabowski, K.R. Subbaswamy, B. Horovitz, Solid State Commun. **34**, 911 (1980); B. Horovitz, Solid State Commun. **34**, 61 (1980); B. Horovitz, Phys. Rev. Lett. **46**, 742 (1980)
49. V. Kiryukhin, B. Keimer, J.P. Hill, A. Vigilante, Phys. Rev. Lett. **76**, 4608 (1996)
50. B. Grenier, L.P. Regnault, J.E. Lorenzo, J. Voiron, J. Bossy, J.P. Renard, G. Dhalenne, A. Revcolevschi, Europhys. Lett. **44**, 511 (1998)
51. M. Horvatić, Y. Fagot-Revurat, C. Berthier, G. Dhalenne, A. Revcolevschi, Phys. Rev. Lett. **83**, 420 (1999)
52. M.H. Rønnow, M. Enderle, D.F. Mc Morrow, L.P. Regnault, G. Dhalenne, A. Revcolevschi, A. Hoser, K. Prokes, P. Vorderwisch, H. Schneider, Phys. Rev. Lett. **84**, 4469 (2000)
53. G.S. Uhrig, F. Schönfeld, J.P. Boucher, M. Horvatić, Phys. Rev. B **60**, 9468 (1999)
54. M.C. Martin, M. Hase, K. Hirota, G. Shirane, Y. Sasago, N. Koide, K. Uchinokura, Phys. Rev. B **56**, 3173 (1997)
55. S. Katano, O. Fujita, J. Akimitsu, M. Nishi, K. Kakurai, Y. Fujii, Phys. Rev. B **57**, 10280 (1998)
56. B. Grenier, J.-P. Renard, P. Veillet, L.-P. Regnault, J.E. Lorenzo, C. Paulsen, G. Dhalenne, A. Revcolevschi, Physica B **259–261**, 954 (1999)
57. R.A. Hyman, K. Yang, R.N. Bhatt, S.M. Girvin, Phys. Rev. Lett. **76**, 839 (1996)
58. J.P. Pouget, Phys. Scripta **17**, 85 (1981)
59. J.P. Pouget, R. Comes, A.J. Epstein, J.S. Miller, Mol. Cryst. Liq. Cryst. **85**, 203 (1982)
60. R. Mélin, Eur. Phys. J. B **18**, 263 (2000)
61. Q. Liu, S. Ravy, J.P. Pouget, I. Johannsen, K. Bechgaard, J. Phys. I France **3**, 821 (1993)
62. Q. Liu, S. Ravy, J.P. Pouget, I. Johannsen, K. Bechgaard, J. Phys. I France **3**, 803 (1993)
63. A. Guinier, *X-Ray Diffraction in Crystals, Imperfect Crystals and Amorphous Bodies* (Dover, 1994)
64. P. Debye, M.R. Anderson, M. Brumberger, J. Appl. Phys. **28**, 679 (1957)
65. J. Kikuchi, T. Matsuoka, K. Motoya, T. Yamauchi, Y. Ueda, Phys. Rev. Lett. **88**, 037603 (2002); J. Kikuchi, S. Ishiguro, T. Matsuoka, K. Motoya, T. Yamauchi, Y. Ueda, Prog. Theo. Phys. (suppl.) **145**, 345 (2002)